PAPER • OPEN ACCESS

Submonolayer and multilayer growth of titaniumoxide-phthalocyanine on Ag(111)

To cite this article: Ingo Kröger *et al* 2016 *New J. Phys.* **18** 113022

IOP Publishing New J. Phys. 18 (2016) 113022 doi:10.1088/1367-2630/18/11/113022

New Journal of Physics
The open access journal at the forefront of physics

Deutsche Physikalische Gesellschaft DPG
IOP Institute of Physics

Published in partnership with: Deutsche Physikalische Gesellschaft and the Institute of Physics

OPEN ACCESS

RECEIVED
9 July 2016

REVISED
9 September 2016

ACCEPTED FOR PUBLICATION
15 September 2016

PUBLISHED
9 November 2016

PAPER

Submonolayer and multilayer growth of titaniumoxide-phthalocyanine on Ag(111)

Ingo Kröger[1,2,3], **Benjamin Stadtmüller**[1,2,4] **and Christian Kumpf**[1,2]

[1] Peter Grünberg Institut (PGI-3), Forschungszentrum Jülich, D-52425 Jülich, Germany
[2] Jülich Aachen Research Alliance (JARA)—Fundamentals of Future Information Technology, D-52425 Jülich, Germany
[3] Present address: Physikalisch-Technische Bundesanstalt, Bundesallee 100, D-38116 Braunschweig, Germany.
[4] Present address: Department of Physics and Research Center OPTIMAS, University of Kaiserslautern, Erwin-Schroedinger-Strasse 46, D-67663 Kaiserslautern, Germany.

E-mail: c.kumpf@fz-juelich.de

Keywords: molecular adsorption, metal-organic interfaces, properties of molecular thin film, titanyl-phthalocyanine

Abstract

For exploiting the full potential of organic materials for future organic electronic devices it is of crucial importance to understand structural and electronic properties of metal-organic interfaces and adsorbate systems, in particular electronic interactions and growth mechanisms. Phthalocyanine molecules represent one class of materials which are very frequently discussed in this context. They feature an appealing tunability in terms of structural, electronic and magnetic properties, simply by exchanging the central (metal) atom or group of atoms. Here we present a comprehensive study of one of the model systems in this field, TiOPc on Ag(111). We discuss structure formation and growth from submonolayer to multilayer films, based on results obtained by electron diffraction, scanning tunneling microscopy, electron energy loss spectroscopy, x-ray standing waves, photoelectron spectroscopy and pair potential calculations. Similar to related metal-phthalocyanine adsorbate systems we find three distinct phases in the submonolayer regime, a disordered gas-like 'g-phase', a commensurate 'c_2-phase' at low temperature, and a 'p.o.l.-phase' consisting of a series of point-on-line structures with continuously shrinking unit cells. For the latter a uniform TiO-up configuration (Ti–O group pointing towards vacuum) was found. Hence, the first-layer molecules form a strong dipole layer, the dipole moment of which is compensated by molecules adsorbing in the second layer at hollow-sites in TiO-down geometry (Ti-O group pointing towards the surface). The Coulomb interaction between the dipole moments in the first and second layer stabilizes this bilayer structure and causes a bilayer-by-bilayer growth mode of molecular films above a thickness of 2 ML. We report the structural properties (vertical adsorption heights, inter-layer distances, inplane orientations and positions) of the molecules in all phases in detail, and discuss the effect of inelastic dynamical charge transfer. Our results contribute to a comprehensive understanding of this interesting adsorbate system and, in comparison with earlier studies on CuPc, H_2Pc and SnPc on Ag(111), we shine new light on the interesting interplay of molecule-molecule and molecule-substrate interactions.

1. Introduction

Obtaining a fundamental understanding of the epitaxial growth of organic semiconductors is crucial for improving molecular based electronic devices such as organic photovoltaics or organic light emitting diodes. Metal-organic interfaces are therefore frequently studied in the literature (see, e.g., [1–9], and references therein). One important aspect in this context is the crystallinity of the organic layers, in particular the size of crystalline grains and the defect densities, since this can significantly influence the mobility of charge carriers and hence affect the efficiency of such devices, as it was recently shown for a zinc-phthalocyanine/C_{60} blend film [10]. It is therefore of crucial importance to understand the properties of the adsorbate–substrate interface and

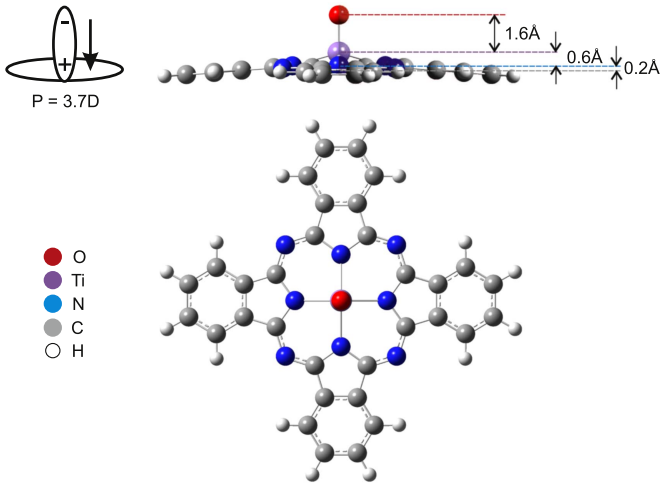

Figure 1. Atomic model of the TiOPc molecule. Due to the central TiO group the molecule exhibits a large vertical dipole moment of 4.6×10^{-29} Cm (3.7 D), as calculated for the gas-phase geometry by DFT (B3LYP, LANL2DZ [24]).

the first organic adsorbate layer, since this layer acts as a template for further growth and frequently determines the properties of the entire organic films [11–16].

Metal-phthalocyanines (MePcs) represent a group of molecules suitable for organic electronics since they are on the one hand good hole conductors, and on the other very versatile in their electronic and geometric properties, depending on the central metal atom (see, e.g., [1, 17] and references therein). Geometric and electronic properties are of course strongly related, as, e.g., recently demonstrated for ZnPc/Cu(111) [18]. The binding energy position of the Zn-derived orbital depends on the vertical Zn–N bonding distance in this case, and can even be pulled into the HOMO-LUMO gap. Since the adsorbate–substrate interaction has a major impact on this intramolecular geometry it can also significantly influence the charge injection barrier.

Another frequently studied aspect is the intrinsic vertical dipole moment (with respect to the molecular plane), which can be tuned by introducing different (metal) central atoms with different electron affinities, or by different molecular geometries. Depending on the size of the metal atom, planar and non-planar molecules can be synthesized, having a more or less considerable dipole moment. Using metal-oxide or -halogenide groups leads to the strongest possible molecular dipole moments. Deposition of these molecules on surfaces opens up the opportunity of tuning work functions and injection barriers by introducing dipole layers at the organic-metallic interface. In a number of recent studies it has been demonstrated that the film epitaxy and the molecular orientation has a big influence on the growth of such dipole layers.

For the molecule under study, TiO-phthalocyanine (TiOPc) (see figure 1), a series of publications by the Ueno/Kera group exists [19–23]. By photoelectron penning ionization spectroscopy and photoelectron spectroscopy (PES) measurements of the valence band and work function they could show that on highly ordered pyrolytic graphite (HOPG) the first layer of molecules grows with the TiO group pointing towards the vacuum ('TiO-up'), building up a well defined dipole layer. The second layer, however, grows with the TiO group pointing towards the substrate ('TiO-down') leading to a very stable bilayer structure and hence to the extinction of the dipole layer.

However, the growth of such molecules on more reactive metal substrates (compared to HOPG) can be very different. In earlier works we have shown that the submonolayer regime of several MePcs on noble metal surfaces (Ag, Cu and Au) is very versatile and shows rich phase diagrams with the molecules in different adsorption geometries [13, 25–29]. For example, the molecular orientation of the non-planar SnPc on Ag(111) changes with coverage in the sub-monolayer regime [13, 25]. While for $\theta \leqslant 0.9$ ML a mix of 'Sn-down' and 'Sn-up' molecules exists, which is well ordered at low temperature (LT), all molecules adsorb in the Sn-down geometry above 0.9 ML. In another study on GaClPc/Cu(111) by Gerlach *et al* [30] the impact of the adsorbate–substrate interaction on the orientation of the molecular dipole was also shown. In that case the chlorine atom is strongly bound to the substrate while the aromatic body of the molecule resides rather far from the substrate ('GaCl-down').

In this context we present a comprehensive study of the monolayer and multilayer growth of TiOPc/Ag(111) in this paper, using complementary methods. We determined the adsorption geometry of the molecules in different structural phases qualitatively and quantitatively, and correlate these results with work function and valence band measurements. The results are compared with studies using different MePc molecules (the planar CuPc and the non-planar SnPc) on the same surface [13, 25, 26] as well as those using the same molecule on

different substrate (TiOPc/HOPG) [19–23]. We are therefore able to present a detailed picture of the different growth modes of planar (CuPc) and non-planar (TiOPc, SnPc) phthalocyanines and the impact of different substrates (Ag(111) and HOPG) on growth mode and electronic structure.

2. Experimental

2.1. Sample preparation

All samples have been prepared and investigated in ultra high vacuum (UHV) with a base pressure below 10^{-9} mbar. The surface of the silver substrate crystal was prepared using a standard procedure by argon ion sputtering (500 eV at $\pm 50^{\circ}$ incident angle, 20 min each) and subsequent annealing at 723 K. For purification the organic material has been sublimated twice before the experiment. For deposition it was evaporated from a home made Knudsen cell with evaporation rates of $\approx$0.5 ML min^{-1}. The sample was held at room temperature (RT) during, but annealed at 513 K after deposition in order to allow the molecules to move across surface steps and guarantee a homogeneous coverage all over the surface. Due to the existence of a metastable bilayer structure this procedure turned out to be crucial in order to remove TiOPc molecules from the second layer. The coverage was determined by monitoring the evaporation rate with a quadrupole mass spectrometer which had been calibrated beforehand using the C1s XPS signal of the monolayer structure as a reference. Note that we define $\theta = 1.0$ ML as the coverage of the densest point-on-line (p.o.l.) structure found in LEED.

2.2. Spot profile analysis—low energy electron diffraction (SPA-LEED)

SPA-LEED is a surface sensitive technique which—compared to conventional LEED—uses a counting detector with a large dynamic range (up to 10^6 cps) and reaches a higher resolution in k-space (the transfer width is usually $>$500 Å). The latter allows a highly accurate determination of unit cells [13, 26, 29]. For TiOPc/Ag(111) films in the submonolayer and multilayer regime we derived superstructure matrices with an uncertainty of $\leqslant$0.04 for the matrix entries by comparing the positions of the LEED spots in experimental and calculated diffraction patterns. The k-space calibration of the SPA-LEED instrument was performed using the well known commensurate superstructure of NTCDA/Ag(111) [31].

2.3. Ultraviolet photoemission spectroscopy

For the ultraviolet photoemission spectroscopy (UPS) investigations we used a He discharge lamp with $h\nu = 21.2$ eV (He–I line) and an hemispherical analyzer. Valence band data were measured under an emission angle of 45°, since the relevant molecular states, the highest occupied and the former lowest unoccupied molecular orbital (HOMO and F-LUMO) yield maximum intensity under these conditions [21, 26, 29, 32, 33]. The measurements were performed at RT with an estimated energy resolution of $\approx$100 meV. Work function measurements using the secondary electron cutoff energy were performed under normal emission. For calibrating the emission angle we used the Shockley surface state of the clean Ag(111) surface leading to an uncertainty of $\pm 1^{\circ}$ [34]. Note that we give relative work function changes before and after deposition, since it is known that the work function of the clean surface often varies with the substrate cleaning procedures. We furthermore mention that SPA-LEED and UPS measurements were performed within the same UHV system on the same sample preparation.

2.4. Scanning tunneling microscopy

Scanning tunneling microscopy was performed in a separated UHV system using an Omicron variable temperature STM at RT and at 110 K (LT). All STM images have been measured in constant current mode. Prior to STM measurements the success of the sample preparation was verified by LEED.

2.5. Normal incidence x-ray standing wave (NIXSW)

The NIXSW technique is a very accurate method to measure the adsorption heights of atoms and molecules above the surface of a crystalline substrate. The method is chemically sensitive since it uses core level photoelectron emission (XPS). Therefore different adsorption heights of any chemically distinguishable atomic species can be detected at a precision of $\approx$0.02 Å. The results can be interpreted in terms of the interaction strength of the adsorbate–substrate bonding as well as of tilting or bending of the molecules. The latter is of special interest in the case of non-planar phthalocyanines such as SnPc [13, 25], GaClPc [30], or TiOPc (this study) since it influences the vertical dipole moment of the molecules.

The NIXSW experiments were performed at the former beamline ID32 at the European Synchrotron Radiation Facility in Grenoble, France. The UHV chamber was equipped with a hemispherical analyzer ($r = 150$ mm) mounted at an angle of 45° relative to the incident beam, a LEED optics and all necessary equipment for sample preparation including a QMS for monitoring the molecular flux during layer deposition.

Table 1. NIXSW multipole correction parameters for the relevant atomic species. All values for Q were derived from NIXSW measurements on incoherent thick films, for which $F^{\mathbf{H}} = 0$ was assumed (see also [25, 40]). Values for Δ were calculated using the code DL_PHASE [41].

	C1s	N1s	Ti2p$_{3/2}$	O1s
Q	0.24(2)	0.22(2)	0.26(2)	0.27(2)
Δ	−0.21	−0.26	−0.21	−0.30

The base pressure during these experiments was $\leqslant 5 \times 10^{-10}$ mbar. The samples were prepared as described above and verified by LEED and XPS regarding lateral structure and coverage, respectively. Since NIXSW is not a standard technique we give a brief introduction to this technique in the following. More detailed descriptions can be found, e.g., in [35–39].

When the Bragg condition for a certain reflection $\mathbf{H} = (hkl)$ is fulfilled, the incident and the Bragg-reflected x-ray wave generate a standing wave field reaching relatively far out above the crystal's surface. The phase ν of the standing wave changes by π when the photon energy (or the diffraction angle) is scanned through the Bragg condition, leading to a spatial shift of the standing wave field by half of the lattice spacing d_{hkl} of the substrate crystal. This changes the amplitude of the standing wave at any position within the crystal (and above its surface) in a very characteristic way. These changes in the XSW amplitudes can be measured at the specific positions of the adsorbed atomic species by recording the XPS yield of the specific atoms. Hence, for any atomic species a photoelectron yield curve $Y(E)$ can be recorded, having a characteristic shape and reflecting the distance of that species from the substrate lattice planes. The measured yield curves can be fitted using

$$Y(E) = 1 + \frac{1+Q}{1-Q}R + 2\sqrt{R} \cdot F^{\mathbf{H}} \cdot \frac{\sqrt{1+Q^2\tan^2\Delta}}{1-Q}\cos(\nu - \Psi + 2\pi P^{\mathbf{H}}), \quad (1)$$

whereby the intensity of the reflected beam R, its complex amplitude $\sqrt{R}$ and the phase ν are derived from fitting the measured reflectivity curve, under consideration of its broadening by the Si(111) double crystal monochromator. The parameters Q, Δ and $\Psi = \tan^{-1}(Q\tan\Delta)$ have been introduced to correct for non-dipolar effects in the photoemission process. For the data presented here, they were either derived from measurements on incoherent films, or taken from literature, see table 1.

The actual result of the XSW analysis is represented by the two parameters coherent position $P^{\mathbf{H}}$ and coherent fraction $F^{\mathbf{H}}$. They are the phase and amplitude, respectively, of the $\mathbf{H}^{\text{th}}$ Fourier component of the spatial distribution of the corresponding atomic species. The coherent fraction is usually interpreted as an 'order parameter' which can have values from 0 to 1, reflecting the degree of vertical order of all the atoms of a certain species. In case of reasonably high coherent fractions, the coherent position $P^{\mathbf{H}}$ can be interpreted as the vertical distance of the atomic species relative to the nearest Bragg plane, in units of the lattice spacing $d_{\mathbf{H}}$ (i.e., it is also a number between 0 and 1). The actual adsorption height $D^{\mathbf{H}}$ of the atomic species in question is related to $P^{\mathbf{H}}$ by $P^{\mathbf{H}} \cdot d_{\mathbf{H}} = D^{\mathbf{H}} \bmod d_{\mathbf{H}}$. Although this relation introduces a mathematical uncertainty for $D^{\mathbf{H}}$, the actual bonding distances can often be obtained easily since usually only one value is physically reasonable.

In case of several distinct adsorption heights, the coherent fraction will also be significantly reduced (even down to a value of zero in extreme cases), although all atoms are located on these different sites without any disorder. Such a case of multiple site adsorption can be treated mathematically by individual coherent fractions $F_m^{\mathbf{H}}$ and positions $P_m^{\mathbf{H}}$ for all of the m distinct adsorption sites. The total coherent fraction and position one would measure in such a case is then given by

$$F^{\mathbf{H}}\exp(2\pi \mathrm{i} P^{\mathbf{H}}) = \sum_{m=1}^{N} o_m F_m^{\mathbf{H}} \exp(2\pi \mathrm{i} P_m^{\mathbf{H}}), \quad (2)$$

where o_m is the occupation of the corresponding adsorption site m, i.e., the percentage of atoms occupying this site. This formula suggests the presentation of NIXSW data in the so-called Argand diagram, that is a visualization of coherent positions and fractions as phases and amplitudes of vectors in a polar diagram. Multiple adsorption heights ($N > 1$) can then simply be dealt with by summing up the individual vectors in this diagram, for an example see section 3.5.2.

For the system under study we have extracted the yield curves from core level spectra for all relevant species. The spectra were measured at 40 different photon energies close to the Bragg energy of the Ag(111) reflection. After background correction they were numerically integrated in order to obtain the $Y(E)$ values. Exemplary XPS data are shown in section 3.3.2.

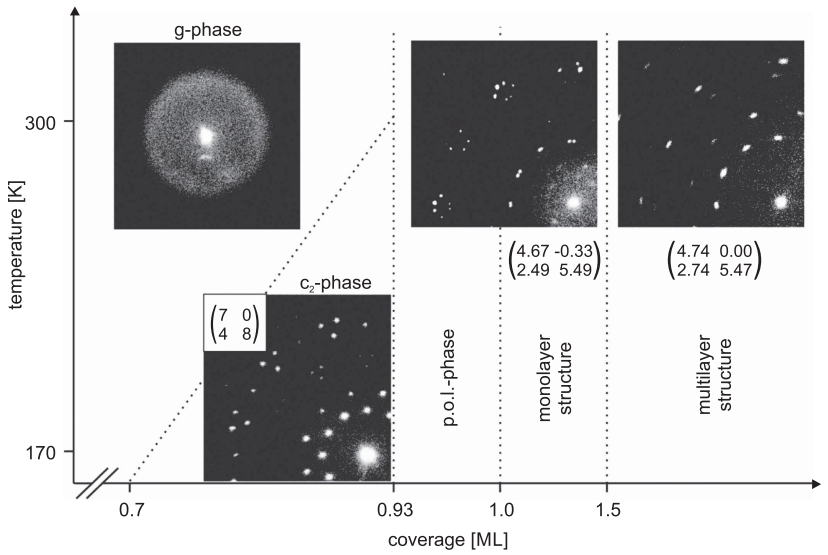

Figure 2. Structural phase diagram of TiOPc/Ag(111). In the submonolayer regime the g-, c_2-, and p.o.l.-phases occur, similar to the system SnPc/Ag(111) [13]. The monolayer structure is present up to ≈1.5 ML, at higher coverages a multilayer structure occurs. The matrices for the c_2-, the monolayer- and the multilayer phases are given. Within the p.o.l. regime the unit cell size is changing continuously, see text and figure 5.

2.6. High resolution electron energy loss spectroscopy (HREELS)

We performed HREELS measurements in order to investigate the vibrational properties of the TiOPc thin films. In particular the modes involving the Ti–O group, which is lying perpendicular to the molecular plane, was in the focus of these experiments, since it is expected to reveal information on the adsorption geometry (i.e., TiO-up or -down).

The HREELS experiments were performed in a separated UHV system at a base pressure below 3×10^{-10} mbar. The system was equipped with a Delta 0.5 HREEL spectrometer, a SPA-LEED optics, and equipment for sample preparation. As in the case of STM and NIXSW the coverages were verified by LEED in order to be able to assign the results correctly. The HREELS experiments we performed in specular geometry (60°) using a beam electron energy of 2.3 eV. The experimental resolution as determined from the FWHM of the specular reflection was 2.5 meV. No beam damage was observed in the HREELS experiments, nor in subsequent SPA-LEED measurements, even after several days of beam exposure. Typical exposure times for the data collection were in the range of 24 h.

3. Results and discussion

At first, we summarize the structural results for the TiOPc/Ag(111) system with coverages of up to 2 ML by presenting the structural phase diagram based on SPA-LEED results. In the following sections, valence band and work function measurements based on UPS are presented, as well as STM and more details of the SPA-LEED investigations, and finally the results of HREELS and NIXSW.

3.1. Structural phase diagram

In the submonolayer regime of TiOPc/Ag(111) three different phases can be identified, a disordered gas-like phase ('g-phase') in the low coverage regime (below 0.7–0.9 ML, depending on temperature), a commensurate c_2-phase existing between 0.7 and 0.93 ML at LT, and a 'p.o.l.' phase at coverages above 0.93 ML. Between 1.0 ML and ≈1.5 ML the LEED pattern of the monolayer-phase is well visible, but it vanishes at higher coverages and is replaced by the pattern of the multilayer structure. Figure 2 summarizes the different regimes of the phase diagram.

We would like to mention that we were never able to reproduce the honeycomb and hexagonal structures reported by Wei *et al* [42]. We believe that this is due to different preparation conditions such as, e.g., the post deposition annealing procedure, and possibly also due to the purity of the organic material being used. We rather find a phase diagram which in the submonolayer regime this very similar to that of SnPc on Ag(111) [13, 25]. In both systems the gas-like g-phase with freely moving and rotating molecules is present. Upon cooling it transforms to the so called c_2-phase, a commensurate phase with two molecules per unit cell, since the molecules condense at well defined adsorption sites. For SnPc in this coverage regime a mixture of Sn-up and

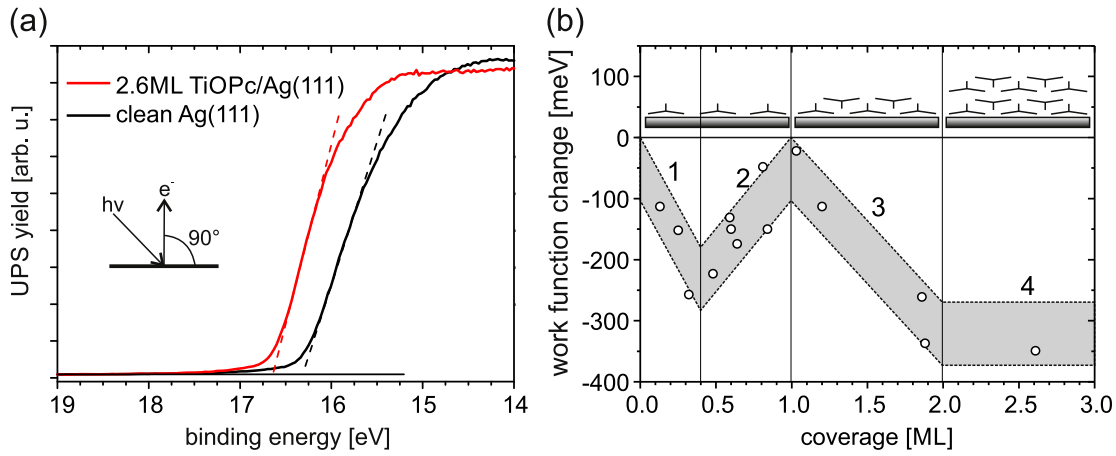

Figure 3. (a) Exemplary data for the determination of the relative work function change from the secondary electron cutoff. (b) Work function of TiOPc/Ag(111) (relative to the clean Ag(111) surface) plotted versus coverage. The inset shows a model for the molecular orientation, which explains the work function changes: Zone 1 and 2: TiOPc molecules build up a dipole layer which increases the work function, however, in zone 1 this effect is overcompensated by the depopulation of the Ag surface state. Zone 3: the second TiOPc layer neutralizes the dipole moment of the first causing a work function decrease. Beside the effect caused by the surface state depopulation (zone 1), this behavior is similar to the case of TiOPc/HOPG, see text. In zone 4 the work function is constant due to the 'bilayer-by-bilayer growth' beyond $\theta = 2$ ML.

Sn-down oriented molecules has been found (in STM and NIXSW), in a disordered manner in case of the (frozen) g-phase, and in a well ordered up-down checkerboard pattern for the c_2-phase. Consequently, no homogeneous dipole layer is formed for this system, in contrast to the TiOPc system, as we demonstrate in the following section. The p.o.l. phase was also found in both systems TiOPc/Ag(111) and SnPc/Ag(111) [13], as well as in CuPc/Ag(111) [26] and H_2Pc/Ag(111) [28]. A continuous change of the unit cell dimensions with increasing coverage has been shown to reflect repulsive intermolecular interaction in all of these systems. We show in the following, that the TiOPc system behaves similarly in this respect.

3.2. Valence band structure, work function and molecular orientation

The change of the work function caused by the adsorption of molecules can be used to gain insight into the orientation and strength of (permanent) dipole moments of the molecules. One relevant example in context with the work presented here is the TiOPc adsorption on HOPG: an increase of the work function by ≈300 meV was reported upon deposition of 1 ML of TiOPc, and explained by the formation of homogeneous 'TiO-up' orientation of the molecules [23]. By deposition of a second TiOPc layer the work function decreases again by approx. the same amount since the 'TiO-down' oriented molecules of the second layer compensate the dipole moment of the first layer. Further deposition causes no significant change in work function, which is explained by a strict bilayer-by-bilayer growth [23].

For TiOPc/Ag(111), the system under study, we have also performed work function measurements using UPS. In figure 3(a) the extrapolated secondary electron cut-offs (dotted lines) for two exemplary measurements are shown, as they were used to determine the work function. We have performed measurements for the coverage regime from submonolayers to multilayers and present the results in figure 3(b). Four different regions can be identified: Between $\theta = 0$ and 0.4 ML (region 1) the work function decreases by ≈200 meV, followed by an increase to about the original value between $\theta = 0.4$ and 1.0 ML (region 2). In region 3, from $\theta = 1$–2 ML the work function decreases again, this time by ≈300 meV, and then it remains unchanged in region 4 (above 2 ML). Apart from region 1 (i.e., the first ≈200 meV decrease) this behavior is identical to the TiOPc/HOPG system described above. Note in particular that extrapolating region 2 towards zero coverage would result in a work function increase of ≈300 meV within the regime of the first monolayer, precisely the same value as observed for TiOPc/HOPG. Hence, the only difference between the two different systems appears to be an additional effect occurring for Ag(111) at very small coverages (region 1). It initially causes a higher work function (by ≈300 meV) at zero coverage and vanishes gradually by deposition of the first 0.4 ML. Angle resolved UPS (ARUPS) measurements have identified a depopulation of the Shockley surface state of the Ag(111) surface to be responsible for this effect [34]: the so called push-back effect, which occurs due to the adsorption of the molecules, leads to a depletion of electrons at the metal surface. With increasing coverage, this continuously pushes the surface state towards lower binding energies, until it becomes completely depopulated at ≈0.4 ML. It also lowers the local potential and explains that the work function is decreasing in this regime. Note that this effect was also observed for other metal surfaces, e.g., for Phthalocyanines on Cu(111), where it is

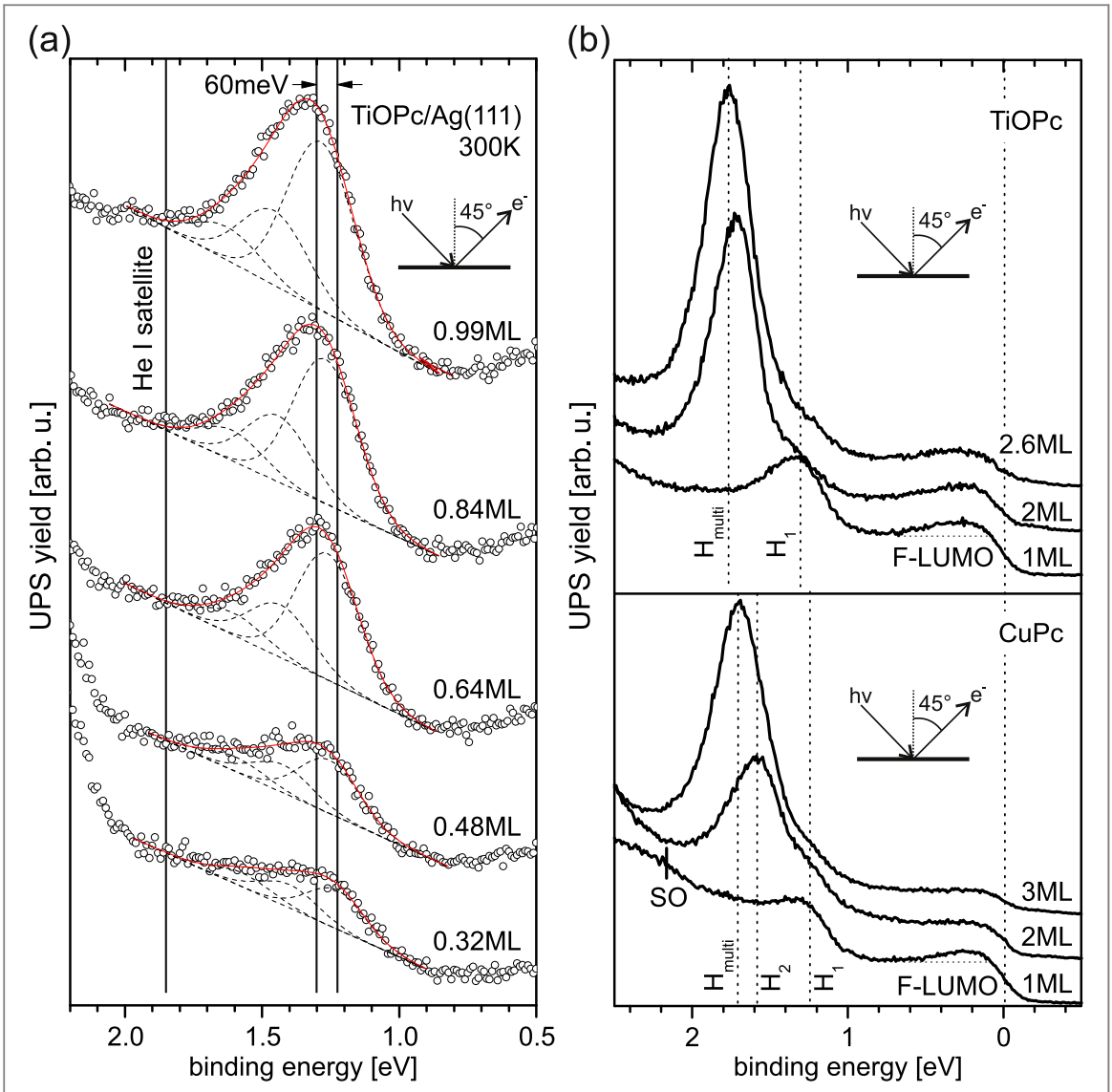

Figure 4. (a) UP spectra of the HOMO region for TiOPc/Ag(111) at different submonolayer coverages. The fit-model with a 2-fold vibronic progression of the HOMO peak is shown as dotted lines, the fit to the data as a red solid line. (b) Comparison of valence band spectra for CuPc/Ag(111) and TiOPc/Ag(111).

even stronger and occurs in a wider coverage regime. In our case, regarding their influence on the work function, the effects of push-back and Shockley surface state depopulation on the one hand, and the formation of the molecular dipole layer on the other, are counteracting. Apparently, in region 1 the first, in region 2 the latter is dominant.

In figure 4 UP spectra for TiOPc/Ag(111) recorded at an emission angle of 45° are shown. Panel (a) illustrates the coverage dependence of the HOMO peak in the submonolayer regime. The asymmetric line shape is well known for phthalocyanine molecules and results from the transitions of the neutral states with vibronic quantum number $\nu = 0$ to the ionic state with $\nu' = 0,\ 1$ and 2 [43]. For fitting we used a model consisting of three Gaussian peaks with a fixed energy separation of 170 meV and a linear background (dotted lines). The gaussian widths as well as the peak heights were free fitting parameters. The data show a continuous shift of the HOMO peak towards higher binding energies by ≈60 meV. For the planar CuPc on Ag(111) a shift of only ≈30 meV was observed in a high resolution UPS experiment performed at 80 K [26]. Therefore this effect cannot be caused solely by the dipole layer formation, but originates at least partly from the adsorbate–substrate interaction, namely the chemisorption of the molecules and the corresponding coverage dependent change of the local potential.

In the multilayer regime a comparison with the TiOPc/HOPG and CuPc/HOPG system can help to evaluate the effect of the dipole layer on the HOMO state [19]. Due to the vacuum level alignment of these physisorbed systems the binding energies (with respect to the Fermi energy) of the molecular states are correlated to the work function change. That results in a strong shift of the TiOPc first-layer HOMO towards

lower binding energies (≈240 meV with respect to the second-layer HOMO peak), in contrast to a negligible shift for the case of CuPc. Similar measurements for TiOPc and CuPc on the Ag(111) surface are shown in figure 4(b). We also observe different binding energies for the HOMO for differently thick films for TiOPc, but the shifts are nearly identical for CuPc and TiOPc, namely ≈470 meV between the 1 ML and the 3 ML film. However, the data shown in figure 4(b) also prove the chemisorptive character of the CuPc and TiOPc adsorption Ag(111), in terms of charge transfer from the surface into the LUMO state [26]. The former LUMO (F-LUMO) is therefore visible in the UPS data as a small peak close to the Fermi level. This is typical for π-conjugated molecules on rather reactive metal surfaces [26, 28, 29, 44–46]. Consequently, the vacuum levels of substrate and molecular layer are no longer aligned, and hence the dipole layer at the interface has a much weaker effect on the binding energy of the molecular orbitals. This is indicated by the almost identical shifts observed for TiOPc and CuPc. The shifts can therefore be correlated with the thickness-dependence of the local potential [47].

We conclude that the work function measurements suggest a similar growth mode (in particular regarding the orientation of the dipole moments of the TiOPc molecules) for both systems TiOPc/Ag(111) and TiOPc/HOPG. The first two layers grow layer-by-layer, the first one with TiO-up, the second with TiO-down orientation. Higher layers are growing bilayer-by-bilayer, each bilayer consisting of TiO-down and TiO-up molecules, so that differently oriented molecules at all times compensate their dipole moments. In contrast to the adsorption on HOPG, on Ag(111) the dipole layer formation has only a minor effect on the binding energies of the of molecular states, since the vacuum level alignment is lifted due to the chemisorptive interaction and the involved charge transfer across the metal-organic interface.

We have also determined the lateral and vertical adsorption geometry in all different phases from SPA-LEED, STM, HREELS and NIXSW data. The measurements result in a conclusive picture of the TiOPc/Ag(111) adsorption, which is presented in the following three sections. We start with discussing the p.o.l. phase at intermediate coverages, since the adsorption geometry of the molecules in this phase is found back in all other phases.

3.3. Adsorption geometries: the p.o.l. phase

3.3.1. SPA-LEED and STM results

The p.o.l. phase was observed in the high coverage regime between 0.93 and 1.00 ML and is (at least) stable in the temperature range from 170 to 300 K. Similar to the adsorbate systems CuPc, SnPc and H_2Pc on Ag(111) [13, 26, 28] the p.o.l.-phase exhibits unit cell parameters which change continuously with increasing coverage. For 27 SPA-LEED measurements within this coverage regime we have identified the superstructure unit cell vectors $\vec{a}$ and $\vec{b}$ and plotted their lengths (given in Angstrøm) and orientations (relative angles to the $[\bar{1}10]$ and $[\bar{1}\,\bar{1}2]$ substrate directions, respectively) in figure 5 (b). In panel (a), an illustration of the corresponding unit cells are plotted on the substrate lattice, indicating that the unit cell is shrinking from an almost rectangular cell at 0.93 ML (dotted lines) to a parallelogram at 1.00 ML (dashed lines). Data points in this diagram represent heads of the corresponding unit cell vectors as obtained from the SPA-LEED measurements. They clearly follow substrate lattice lines during the continuous shrinking of the cell, indicating that this phase is indeed of the p.o.l. lattice type.

The matrix of the largest superlattice cell found for TiOPc/Ag(111) (205.6 Å^2) is $\begin{pmatrix} 4.94 & -0.06 \\ 2.74 & 5.72 \end{pmatrix}$ at a coverage of 0.93 ML. This finding represents a significant difference to the CuPc/Ag(111) system: there, the largest cell was found at a significantly lower coverage of 0.89 ML (217.0 Å^2) [26], corresponding to the commensurate limit of the superlattice with the matrix $\begin{pmatrix} 5 & 0 \\ 3 & 6 \end{pmatrix}$. Hence, the disorder-order transition from the g-phase to the p.o.l.-phase is retarded for the TiOPc growth compared to CuPc, which might be explained by an additional intermolecular repulsion due to relatively strong dipole moments of the (TiO-up oriented) TiOPc molecules. The same tendency (in weaker form, in accordance with a weaker molecular dipole moment) can be observed for SnPc/Ag(111) [13].

Figure 5(c) shows an empty states STM image of TiOPc molecules in the p.o.l.-phase at a coverage of ≈0.94 ML. The tunneling contrast shows the well known cross-like shape of phthalocyanine molecules with a clear protrusion in the center. All molecules on the surface show the same tunneling contrast, indicating that the unit cell contains only one flat lying molecule, but of course in different rotational domains.

A small number of 'defect molecules', not showing the central protrusion but appearing planar, were also found. A comparison of STM scans through the centers of both types of molecules is shown in figure 5(d), indicating an apparent height of the protrusion of ≈0.7 Å. Since this protrusion is visible for different bias voltages and polarities, it can be interpreted as an indication for a TiO-up geometry, although maybe not as a proof. It has been shown earlier that the molecules CoPc and CuPc—both being planar, also after adsorption on a Au(111) surface—exhibit a central protrusion with an apparent height as large as 2.5 Å [48], which

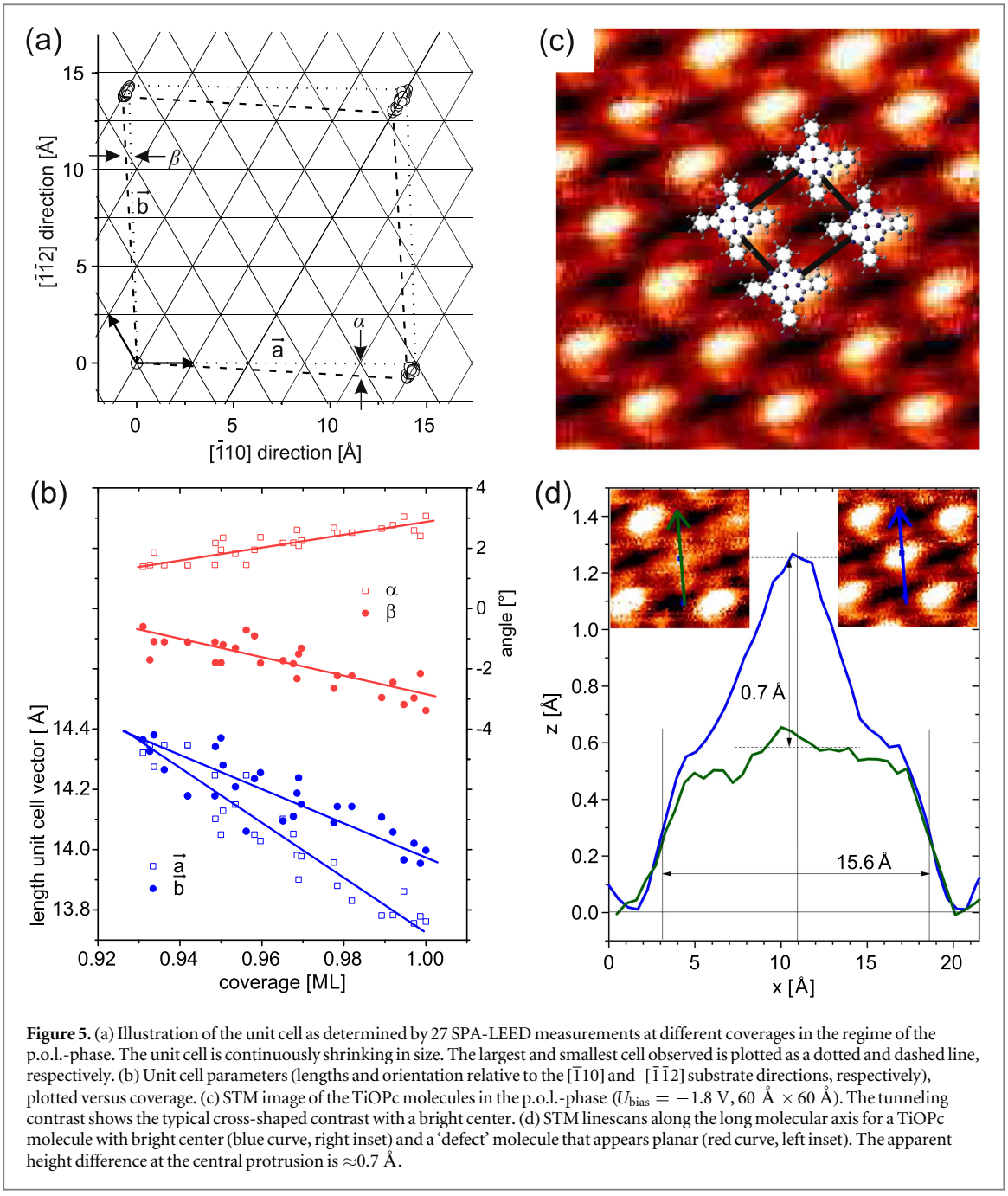

Figure 5. (a) Illustration of the unit cell as determined by 27 SPA-LEED measurements at different coverages in the regime of the p.o.l.-phase. The unit cell is continuously shrinking in size. The largest and smallest cell observed is plotted as a dotted and dashed line, respectively. (b) Unit cell parameters (lengths and orientation relative to the $[\bar{1}10]$ and $[\bar{1}\bar{1}2]$ substrate directions, respectively), plotted versus coverage. (c) STM image of the TiOPc molecules in the p.o.l.-phase ($U_{bias} = -1.8$ V, 60 Å $\times$ 60 Å). The tunneling contrast shows the typical cross-shaped contrast with a bright center. (d) STM linescans along the long molecular axis for a TiOPc molecule with bright center (blue curve, right inset) and a 'defect' molecule that appears planar (red curve, left inset). The apparent height difference at the central protrusion is ≈0.7 Å.

demonstrates that the contrast of the Pc molecules is strongly dominated by the density of states of the d-orbitals, not by the geometric height of the molecules. More conclusive information about adsorption heights are obtainable by NIXSW experiments, as presented in the following.

3.3.2. NIXSW results

We have performed NIXSW measurements for an adsorbate layer within the p.o.l.-regime, namely at a coverage of 0.95 ML. Exemplary core level spectra demonstrating the background subtraction procedure are shown in figure 6. For C1s, Ti2p$_{3/2}$ and O1s a linear background approximation was used. However, the vicinity of the N1s peak is dominated by three Ag plasmon peaks, and therefore a significantly larger binding energy range had to be measured in order to be able to fit the background with three gaussian peaks with constraining their widths and height ratios. For details of the background treatment for this species see [25, 26].

Beam damage turned out to be a crucial issue for this adsorbate system. In repeated very short XSW scans we observed a significant decrease of the coherent fraction after exposure times of ≈10 min. We therefore limited the time for each XSW measurement to ≈5 min and changed the illuminated spot on the crystal surface after each scan. This lead to relatively poor signal to noise ratios in the individual spectra, in particular for Ti2p$_{3/2}$,

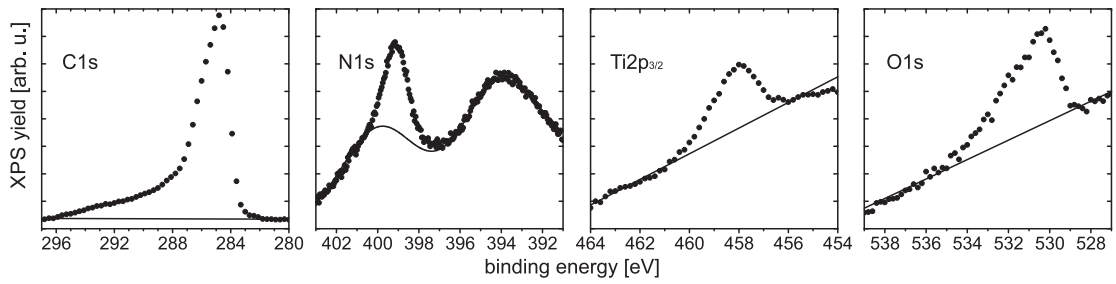

Figure 6. Exemplary core level spectra of all species investigated. A linear background was considered for C1s, $Ti2p_{3/2}$ and O1s. For N1s the background is modulated by three Ag plasmon peaks for which three gaussian peaks were used for fitting.

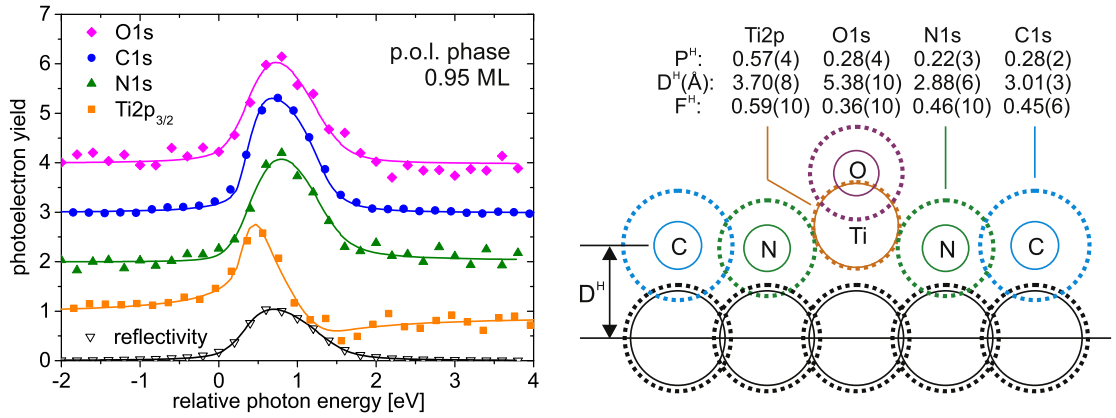

Figure 7. NIXSW data (left) and corresponding adsorbate model (right) for 0.95 ML TiOPc on Ag(111) at RT. Experimental yield data are shown with corresponding fitted curves, as well as one exemplary reflectivity curve (lowermost curve). The fit parameters (coherent position $P^{\mathbf{H}}$ and coherent fraction $F^{\mathbf{H}}$) are listed in the right. In the model, circles with solid lines denote covalent, those with dotted lines van-der-Waals bonding radii of the individual atoms [49, 50].

N1s, and O1s. For the XSW analysis we therefore summed up the spectra of several XSW scans (up to 30) recorded at different spots on the sample surface before fitting.

Figure 7 shows the results for the 0.95 ML TiOPc p.o.l. layer. The yield curves for all atomic species are plotted in the left panel, together with an exemplary reflectivity curve. The corresponding fit results for the coherent position $P^{\mathbf{H}}$ and coherent fraction $F^{\mathbf{H}}$ are listed in the right panel. When considering previous knowledge obtained from NIXSW measurements of adsorbed aromatic molecules on Ag(111) [13, 25, 26, 28, 40, 51–53] and from the intramolecular bond length of the gas phase geometry, the fit results can be unambiguously interpreted as adsorption heights relative to the topmost bulk lattice plane. This is illustrated in the real space model shown in the right part of figure 7. Given uncertainties are typical estimates derived from previous experiments [13, 25, 26, 28, 40].) Note that the coherent fractions obtained for these measurements are relatively low (0.4–0.6) for most species, indicating a rather high degree of disorder in the molecular films, which might already be due to nascent radiation damage. In particular the oxygen is affected, since this species is not solidly embedded in the molecule but only bonded to the Ti atom. However, since a moderate radiation damage will not be the reason for additional discrete adsorption sites (heights) of any of the individual atomic species, it is expected to only reduce the coherent fraction noticeably, but not influence the coherent positions significantly.

The NIXSW data clearly proves a 'TiO-up' adsorption geometry with the Ti–O group pointing towards the vacuum, as it was already suggested by the work function measurements. The intramolecular vertical distances are $d_{\mathrm{O-Ti}} = 1.68$ Å and $d_{\mathrm{Ti-N}} = 0.82$ Å, and hence very close to those for the gas phase geometry (1.6 Å and 0.6 Å, respectively, see figure 1). The adsorption height of the aromatic body of the molecule (carbon and nitrogen atoms) above the Ag surface lies in the range of 2.88–3.01 Å, which is significantly smaller than the sum of the corresponding van-der-Waals radii. This indicates a chemisorptive adsorbate–substrate interaction similar to SnPc/Ag(111)[25], CuPc/Ag(111)[26] or H_2Pc/Ag(111)[28], and is consistent with the observation of the F-LUMO state in UPS data. The chemisorptive character is further confirmed by the almost planar aromatic

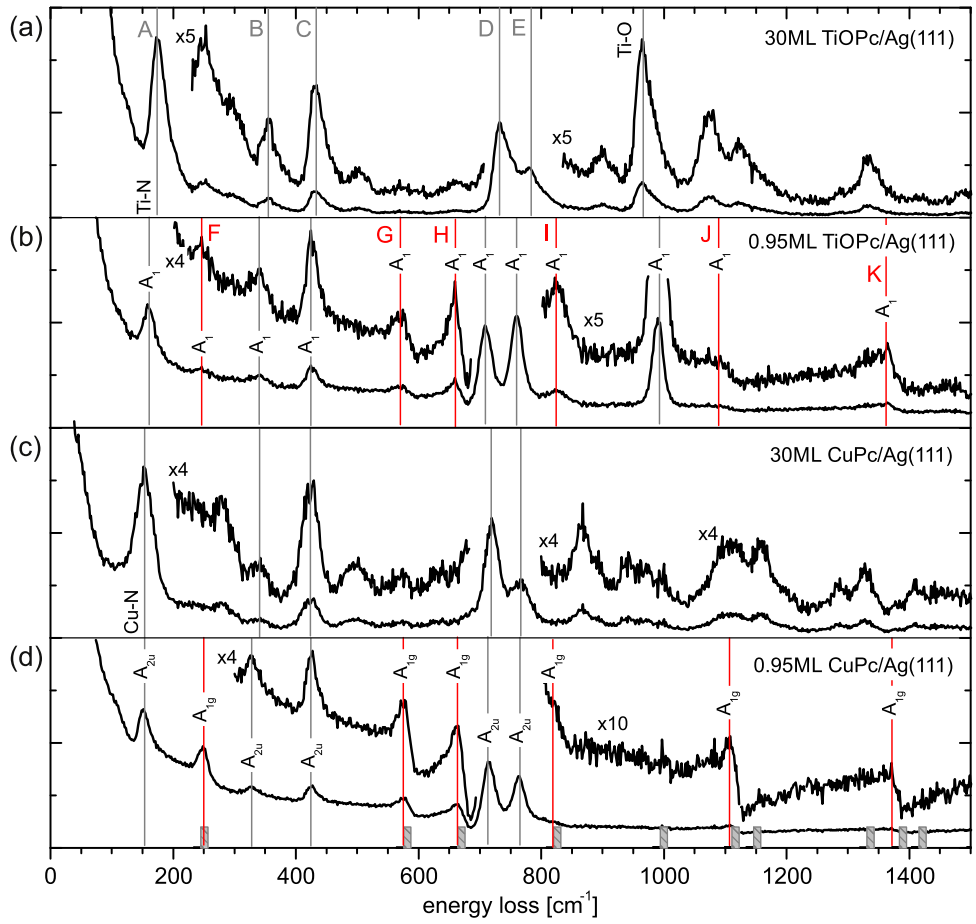

Figure 8. HREEL spectra of (a) an amorphous multilayer of TiOPc (b) a TiOPc p.o.l.-phase, (c) an amorphous multilayer of CuPc and (d) a CuPc p.o.l.-phase. The dominant IR active out-of-plane modes A-E (indicated by gray lines) are similar in all spectra. For TiOPc the strong Ti–O stretching mode can also clearly be identified. Surface enhanced modes caused by inelastic dynamical charge transfer (IDCT) are found in the submonolayer spectra (modes F–K marked by red lines in panel (b) and (d)) and can be identified by their asymmetric line shape. Totally symmetric A_{1g} modes of CuPc calculated by DFT from Liu *et al* [54] (see also table 2) are shown as bar chart on the abscissa for comparison.

body (d_{N-Ag} is equal to or even smaller than d_{C-Ag}), which is in contrast to the gas phase geometry and indicates a rather strong bonding between the nitrogen atoms and the substrate.

We can conclude from the NIXSW data that the 'TiO-up' orientation of the TiOPc molecules on Ag(111) in the p.o.l.-phase, which was suggested by the work function measurements, is correct, and that the bonding of the molecule to the substrate via its aromatic body is chemisorptive, in agreement with PES experiments. A comparison of the adsorption heights determined in NIXSW ($d_{Ti-N} = 0.82$ Å) and the apparent height of the central protrusion of the molecules seen in STM (≈0.7 Å) suggests that it is actually the titanium atom (probably one of its d-orbitals) which is seen in STM.

3.3.3. HREELS results

HREELS has been performed for both the TiOPc and the CuPc/Ag(111) system, and due to the well characterized adsorption geometry in the p.o.l.-phase it could be interpreted rather straightforwardly. At first we have recorded reference data for thick amorphous films with a nominal coverage of ≈30 ML, deposited on a cold substrate (113 K), for which no ordered structure was visible in LEED (see figures 8(a) and (c)). In these amorphous films the molecules should be randomly oriented and hence the HREEL spectra should not be affected by surface selection rules, so that all infrared-active in-plane and out-of-plane modes should be visible. A comparison of these data for CuPc and TiOPc in figures 8(a) and (c) reveals almost identical vibrational properties of both molecules, apart from one strong line at 965 cm^{-1} for TiOPc. This line can therefore be identify as the Ti–O stretching mode. The rest of the spectrum, which contains all other modes corresponding to the aromatic body of the molecule, is dominated by five strong out-of-plane modes labeled A–E and marked with gray lines in figure 8: A: 174 cm^{-1} and 151 cm^{-1} (TiOPc and CuPc, respectively), B: 356 cm^{-1} and 340 cm^{-1}; C: 434 cm^{-1} and 423 cm^{-1}; D: 732 cm^{-1} and 719 cm^{-1}; and E: 782 cm^{-1} and 766 cm^{-1}. These modes were identified as out-of-plane modes since they are still observable in the submonolayer regime

Table 2. Table of totally symmetric Raman modes (A_{1g}), calculated by DFT (Liu *et al* [54]) for CuPc in the gas-phase (first column). The measured IDCT-enhanced vibrational modes of the CuPc submonolayer on Ag(111) (F–K, second column) coincide very well with the A_{1g} modes. Abbreviations: Porph. = porphyrine ring, N_m = nitrogen connecting isoindole groups, Ben. = benzene ring, Iso. = isoindole group, Pyr. = pyrrole ring, bre. = breathing, str. = stretching, exp. = expanding, ipb = in-plane bending.

$CuPc^{DFT}_{A_{1g}}$ [54]	$CuPc_{exp}$	Type of mode
250 cm^{-1}	F: 250 cm^{-1}	Porph. bre.
581 cm^{-1}	G: 573 cm^{-1}	Porph. bre.; N–Me str.; Ben. exp.
669 cm^{-1}	H: 663 cm^{-1}	C–N_m–C ipb; Iso. exp.
825 cm^{-1}	I: 817 cm^{-1}	N–Me and Pyr. str.; Ben. exp.; C–N_m–C ipb
999 cm^{-1}	—	C–H ipb; Ben. exp.
1116 cm^{-1}	J: 1105 cm^{-1}	C–H ipb; Iso. and N–Me str.
1151 cm^{-1}	—	C–H ipb
1336 cm^{-1}	—	Iso. and N–Me str.; C–H and C–N_m–C ipb
1389 cm^{-1}	K: 1372 cm^{-1}	Pyr., C–C and N-Me str.; C–N_m–C and C–H ipb
1421 cm^{-1}	—	C–N_m–C str.; Pyr. exp.; C–H ipb

(figures 8(b) and (d)), where in-plane modes are strongly damped by the surface selection rule. Mode A can be assigned to the metal-N stretching mode, the modes B and C are out-of-plane deformation modes of the macrocycle. Mode D and E are out-of-plane C–H stretching modes that are very characteristic for aromatic molecules (e.g., for PTCDA, see [4, 55–58]). Similar vibrational properties have also be observed for ZnPc/Ag (110) [59] and CuPc/Au(111) [60]. Note that for mode assignment we have performed DFT calculations using the Gaussian03 package (B3LYP, Basis set: LANL2DZ) [24] which resulted in a good agreement with the previous work of Liu *et al* [54].

When comparing HREEL spectra obtained for the p.o.l.-phase with the reference data recorded for multilayers it becomes obvious that some of the peaks are shifted. Most interestingly, the Ti–O stretching mode is shifted to higher (from 965 cm^{-1} to 991 cm^{-1}), the N–Ti stretching mode to lower wavenumbers (from 174 cm^{-1} to 161 cm^{-1}), whereas the Cu–N stretching mode remains unchanged. This observation indicates a strengthening of the Ti–O bond and a weakening of the N–Ti bond upon adsorption of TiOPc, whereas the copper atom within the CuPc molecule remains unaffected. It might be correlated with the LDOS of the F-LUMO being located at the metal atom for the case of TiOPc, in contrast to CuPc/Ag(111) [61].

There are some other strong lines labeled F–K in the HREEL spectra of the p.o.l.-phase, which do not correspond to out-of-plane modes. At first sight this is surprising, since NIXSW and STM data showed that the molecules adsorb in a flat-lying geometry on the surface, so that all these in-plane modes should be suppressed by the surface selection rule. Note that these lines F–K show a characteristic asymmetric lineshape, the so-called Fano-lineshape, which is typical for weakly chemisorbed aromatic molecules. It is an indication for a strong electron-phonon coupling and originates from the inelastic dynamical charge transfer (IDCT) at the organic/metallic interface [57].

An IDCT can occur under two conditions, namely (1) that a metallic orbital of the adsorbate is strongly coupled to substrate states and forms a hybrid state, and (2) that vibrational modes couple very efficiently to this metallic hybrid state. The first condition is fulfilled by the F-LUMO, which in both cases (CuPc/Ag(111) [26] and TiOPc/Ag(111), see figure 4(b)), involves the metal atom of the molecule. The latter is fulfilled since the F-LUMO is partially filled, which allows a strong electronic reaction on any vibration involving the binding energy position of the F-LUMO (in contrast to weakly interacting systems as, e.g., CuPc/Au(100) [60]). Therefore the IDCT can occur in these systems, leading to a dynamical dipole moment perpendicular to the surface, which in turn is the reason for the totally symmetric (usually only Raman active) modes to become IR active and hence being visible in the HREEL spectra. For CuPc these modes are of A_{1g} symmetry. The values calculated by Liu *et al* using DFT [54] are shown in figure 8 as bar charts and listed in table 2. The A_{1g} modes at 250 cm^{-1}, 581 cm^{-1}, 669 cm^{-1}, 825 cm^{-1}, 1116 cm^{-1} and 1389 cm^{-1} coincide very well with the modes F–K and hence confirm their origin in the IDCT. For TiOPc these modes are of A_1 symmetry and hence intrinsically IR active. But due to the IDCT the IR activity is strongly enhanced in the p.o.l. phase, as can be seen from a comparison with the multilayer spectrum.

Summarizing all results of the p.o.l. phase we can state that all experimental methods applied (that are UPS, work function measurements, SPA-LEED, STM and NIXSW as well as HREELS) indicate that the TiOPc molecules adsorb flat-lying in a 'TiO-up' geometry. The layer is very well ordered and has one molecule per surface unit cell. SPA-LEED measurements show a decreasing unit cell size with increasing coverage, indicating a repulsive intermolecular interaction (similar to other MePc molecules on Ag(111)). NIXSW and UPS indicate a chemisorptive character of the adsorbate substrate interaction (a partially filled F-LUMO and an adsorption

height of ≈3.0 Å, smaller that van der Waals bonding distances), which is confirmed by the interface dynamical charge transfer (IDCT) observed in HREELS (via some Raman active totally symmetric modes which become IR active due to the IDCT). The latter technique also allowed us to identify the Ti–O stretching mode (at 991 cm^{-1}), and indicated that the N–Ti bond is weakened while the Ti–O bond is strengthened by the interaction of the TiOPc molecule with the Ag surface.

3.4. Adsorption geometries: the g- and c_2-phase

The g- and c_2-phases exist at smaller coverages (below 0.93 ML) at RT and LT, respectively. It is observed that the transition temperature between these two phases increases from values below 130 K at 0.5 ML to (approximately) RT at 0.93 ML (see figure 2). This behavior is very similar to the SnPc adsorption on Ag(111), and differs from the systems CuPc and H_2Pc/Ag(111) only by the fact that the c_2-phases of SnPc and TiOPc phases have two inequivalent molecules in the unit cell while those of the c-phases of CuPc and H_2Pc contain only one. For SnPc/Ag(111) it was also shown that the two inequivalent molecules in the c_2-phase are differently oriented, they form a well ordered checkerboard pattern of 'Sn-down' and 'Sn-up' molecules, and that they occupy different adsorption sites on the Ag(111) substrate [25]. For the g-phase a similar disordered mixture of 'Sn-down' and 'Sn-up' molecules was found, while for the p.ol.-phase all molecules adsorb in the 'Sn-down' geometry.

A similar behavior suggests itself for TiOPc/Ag(111), since this molecule is also non-planar, just like SnPc. The unit cell parameters of both the TiOPc c_2- and p.o.l.-phase (see figure 9(a)) are very similar to those for SnPc/Ag(111). In particular, as clearly seen in the STM image in figure 9(b), two inequivalent molecules are present in the c_2 phase of TiOPc (upper right half of the image), just as in the case of SnPc. In the lower left a domain of the p.o.l. phase is visible. STM images showing the coexistence of these two phases can be observed for coverages very close to 0.93 ML in such regions of the crystal where the local coverage differs slightly on different terraces. The STM image shows clearly an uniform ('TiO-up') configuration (indicated by the bright protrusion in the center for the molecules) in the p.o.l. phase. In the c_2-phase, some molecules show identical contrast, suggesting the same 'TiO-up' configuration, but others have a more homogeneous contrast without that strong central protrusion.

Further insight can be gained from HREELS, since the Ti–O out-of-plane stretching mode should be very sensitive for conformational changes of the central group of the molecule. Figure 9(c) shows a comparison of the corresponding spectra of p.o.l.-, c_2-phase and g-phase. The spectra are normalized to the height of the C–H out-of-plane stretching mode at 761 cm^{-1} in order to compensate for different coverages. It is remarkable that the Ti–O stretching mode does not change its position but only its intensity, which is reduced by a factor of two for the g -and c_2-phases compared to the p.o.l.-phase. This indicates that no significant change in the Ti–O bonding strength (and length) occurs, but that the number of (visible) oscillators is reduced. Both is in accordance with the STM images showing identical contrast for one of the c_2-phase molecules and the p.o.l-phase molecules. We can conclude that these molecules have identical adsorption geometries, namely 'TiO-up'.

The question is, what the configuration of the other molecule in the c_2-phase is. Since no other frequency-shifted line in the HREEL spectra was found, the conclusion might be that the O-atom has dissociated from the molecules of this type. However, it turned out that a c_2-phase sample can be transformed to an intact layer of the p.o.l.-phase (i.e., with all molecules showing an identical 'TiO-up' contrast in STM) by increasing the TiOPc coverage slightly to values above 0.93 ML and warming up the sample to RT. Since only a small amount of molecules has to been added for this phase transition (much less than half of the original coverage), the oxygens of the TiOPc molecules in question must still be there, and dissociation can safely be excluded. Apparently, the change in intensity of the of HREELS line must originate from surface selection rules, which might be caused by a change of the Ti–O bond angle relative to the surface. We have tried to verify this assumption in NIXSW and considered both a tilt of the Ti–O group with respect to the rest of the molecule as well as a tilt of the entire molecule, as suggested by Wei *et al* for different lateral structures [42]. While the latter is clearly not compatible with the NIXSW results, we also tested a more dedicated analysis of the NIXSW data in order to check for the first assumption. We tried to resolve two (or more) different adsorption heights for Ti atoms (and also for O). However, this analysis did not result in a firm conclusion since too many degrees of freedom (coherent positions and fractions for two different adsorption sites, precise ratio of both molecular species in the g-phase, and possibly some adsorption of water in the LT measurements) made the analysis of the data unreliable. Hence, the conclusion drawn from STM and HREELS—namely that the Ti–O group of the second molecular species in the c_2-phase, which exhibits a rather flat STM contrast, is not oriented vertically to the surface but significantly tilted and therefore becomes invisible in HREELS—remains somewhat speculative. However, we can firmly conclude that the other TiOPc molecule of the c_2-phase, and all molecules in the p.o.l.-phase, are oriented with their Ti–O group pointing towards the vacuum ('TiO-up adsorption geometry').

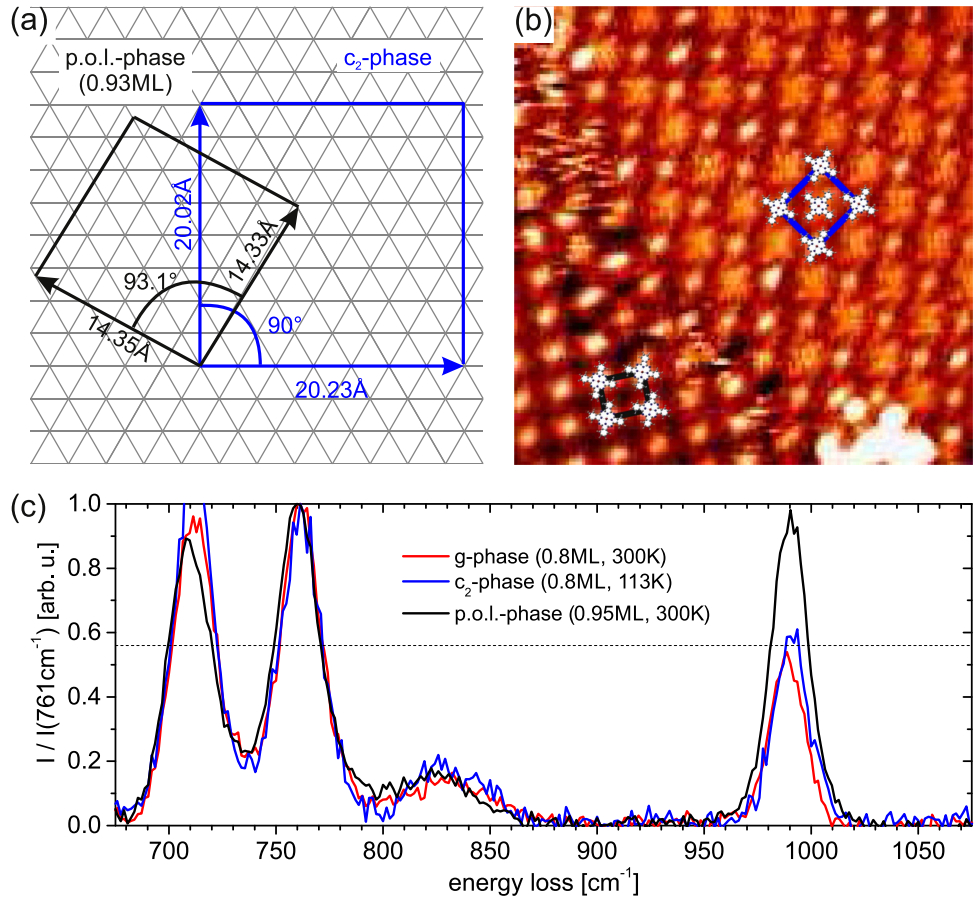

Figure 9. (a) Unit cells of the c_2-phase and a p.o.l.-phase of TiOPc on the Ag(111) surface lattice, illustrated in blue and black, respectively. (b) STM image (150 Å × 150 Å) of a sample exhibiting a coexistence of p.o.l.- (lower left) and c_2-domains (upper right). For the c_2-phase, two inequivalent molecules per unit cell can be identified. (c) HREEL spectra for the p.o.l.-, the c_2- and the g-phase in the region of the Ti–O out-of-plane stretching mode (991 cm^{-1}). The data are normalized to the maximum of the C–H out-of-plane stretching mode at 761 cm^{-1}. The intensity of the Ti–O mode is reduced to ≈55% in the g- and c_2-phase compared to the p.o.l.-phase.

3.5. Adsorption geometries: the multilayer structure

For the TiOPc/Ag(111) bilayer structure we have obtained structural data using SPA-LEED, STM and NIXSW, and also performed pair potential calculations to confirm the high energetic stability of this phase.

3.5.1. SPA-LEED and STM results

The multilayer structure of TiOPc has been observed in LEED for coverages above 1.5 ML. This is significantly earlier than for CuPc/Ag(111), where clear changes in the LEED pattern occur only above 3 ML. In figures 10(a) and (b) the corresponding LEED patterns are shown for both structures, together with an illustration of the unit cell on the Ag(111) surface lattice. The unit cells are similar in size, but also significantly distorted in the case of CuPc. Note that these multilayer structures are observed (in LEED) without significant changes for coverages up to 30 ML.

A first indication of the extraordinarily high stability of the bilayer phase can be seen in figure 10(c). It shows a conventional LEED pattern of a closed bilayer structure of TiOPc/Ag(111) (i.e., rather precisely a coverage of 2.0 ML, as determined by XPS) which was prepared from desorption of a thick multilayer by annealing to 568 K for 160 min. This way of sample preparation produces a bilayer of excellent crystalline quality and extremely large domains on the crystal surface. In this case the domains were so large that in conventional LEED only *one* of the six rotational and mirror domains was visible. Note that the size of the illuminated spot on the sample in our LEED instrument is in the millimeter range.

Figure 10(d) shows an STM image of second-layer molecules adsorbed on a closed monolayer structure, i.e., an incomplete TiOPc bilayer structure. The second-layer molecules appear as white cross-like protrusions on a carpet of dark-red first-layer molecules underneath. Molecules are marked with white (first) and black (second layer) symbols in the lower part of the figure, and white lines indicate the unit cell. First layer molecules are rotated by ≈35° to the unit cell vector (and hence to the high symmetry directions of the substrate, see

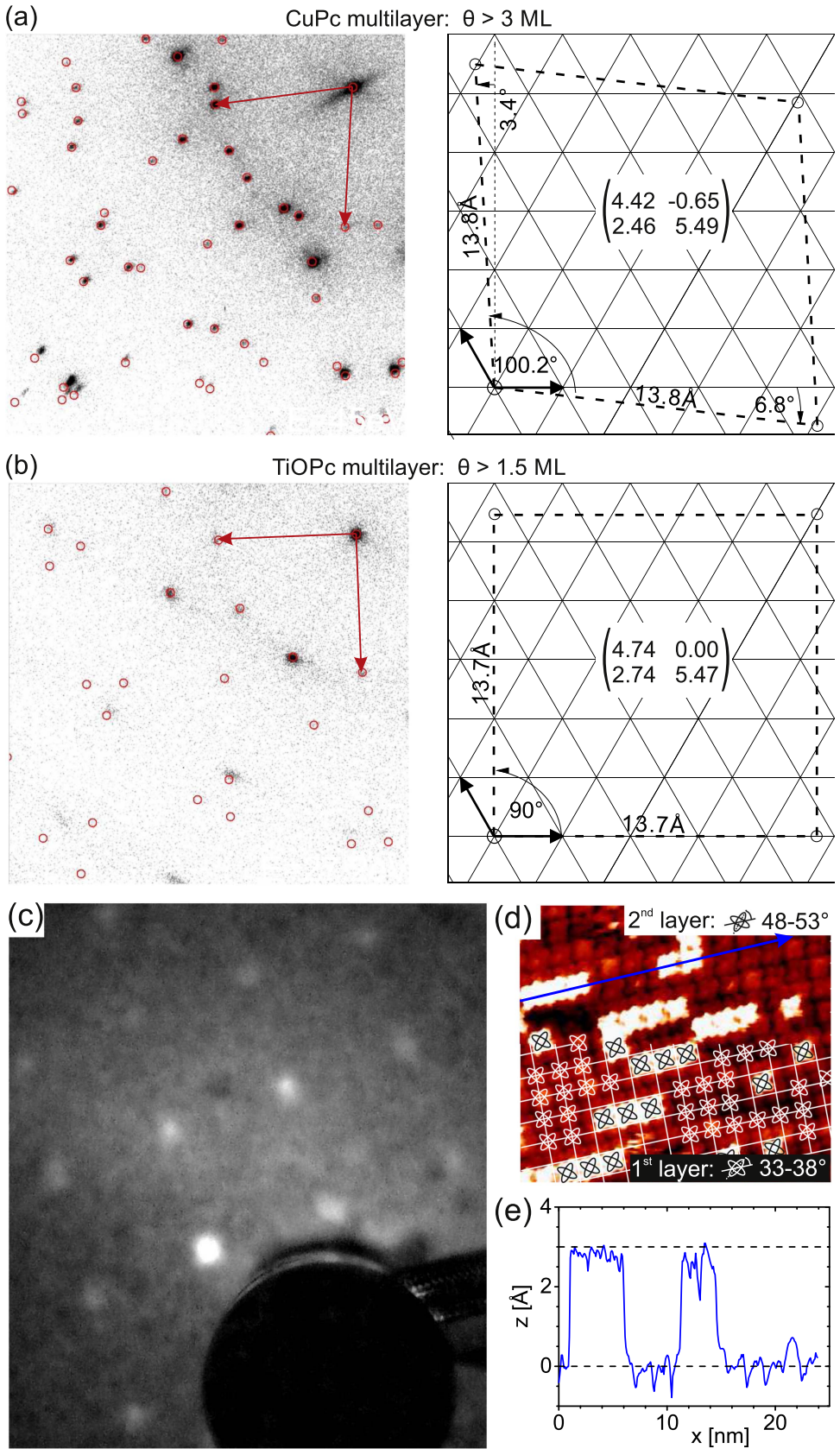

Figure 10. (a) and (b) SPA-LEED pattern of the CuPc and TiOPc multilayer structure on Ag(111), respectively. Red circles mark calculated peak positions according to the unit cells matrices given on the right. The corresponding lattice parameters are drawn on an Ag(111) surface lattice. (c) LEED pattern from a millimeter-sized single domain TiOPc/Ag(111) bilayer film. (d) STM image of a partial bilayer structure of TiOPc/Ag(111) ($U_{bias} = 1.8$ V, 18 nm × 16 nm). Molecules in the first and second layer show dark red and white contrast and are labeled by the white and black symbols, respectively. White lines indicate the unit cell. The blue line indicates the position of the linescan shown in (e). The apparent height difference between the molecules in first and second layer is ≈3 Å.

figure 10(b)). This enables an alignment of one pair of molecular wings rather precisely along the silver atomic rows, which indicates the influence of the adsorbate–substrate interaction.

As illustrated in figure 10(d), second layer molecules are located at hollow sites above four first-layer molecules with an azimuthal alignment of ≈50°, i.e., their wings point towards the centers of the underlying first layer molecules. Obviously, this arrangement enables the suggested 'TiO-up/TiO-down' bilayer structure, which was discussed in context with the work function measurements (see above). Oppositely oriented vertical dipoles compensate each other very efficiently, which gives rise for a rather strong attractive interaction between the corresponding molecules. Note that the protrusion of the first layer molecules is not visible in figure 10(d) only due to scaling of the height axis. A line scan through molecules in the first and second layer is shown in panel (e) of this figure, indicating an apparent height difference of ≈3 Å.

3.5.2. NIXSW results

NIXSW measurements were performed on the bilayer structure, the LEED pattern of which is shown in figure 10(c). Since in our case core level shifts of the same atomic species in different layers are not large enough to disentangle the corresponding XPS yields, we can only obtain an averaged signal from both layers of the bilayer structure, i.e., we have to deal with a special case of multiple site adsorption. Therefore, the adsorption heights of the second layer molecules can only be determined under the assumption that the first layer is not (significantly) changed by the adsorption of the second. This assumption is not precisely correct, as, e.g., demonstrated for CuPc/PTCDA/Ag(111) in [62], and hence an (additional) uncertainty in the range of ≈0.1 Å has to be assumed for this analysis.

As mentioned in section 2.5, multiple site adsorption is dealt with by vector sums in an Argand diagram. In this specific case, the Argand vectors representing the NIXSW results of the second-layer species can be calculated by subtracting the vectors found for the p.o.l.-phase (see section 3.3.2) from those for the bilayer structure. The analysis of the plain bilayer data ('sum'-yield curves, average from both layers) is shown in figure 11(a), coherent fractions and positions are also given as numbers. In panel (b) we display the vector-sum analysis of the plain data: circles and triangles represent the measurements for the bilayer structure and the p.o.l.-structure, respectively (see also figure 7). The symbols mark the positions of the heads of the corresponding Argand arrows, whereby phase angle and length of the vectors in turn represent the coherent position and fraction, respectively. The squared symbols, which are obtained by the vector difference of bilayer (circles) and p.o.l. results (triangles), mark the resulting Argand vector for the second layer of the TiOPc bilayer structure. Note that according to equation (2) the lengths of the vectors used in the vector sum for the first and second layer is $o_m F_m^{\mathbf{H}}$, i.e., they are multiplied with the occupation of the corresponding sites. In our case these occupations of both adsorption sites are 50% each, since an equal number of molecules is located in both layers. The measured coherent fraction of the p.o.l.-phase must therefore be multiplied with 0.5 for drawing the corresponding Argand vector, the resulting second-layer vector must be divided by 0.5 in order to obtain the correct coherent fraction for this site. In figure 11(c) we present the resulting adsorptions heights and coherent fractions, and a model illustrating the vertical structure of the bilayer film.

The resulting adsorption model clearly confirms the 'TiO-up/TiO-down' geometry suggested above. The intramolecular vertical distances between the atomic species of the second-layer molecules are $d_{\mathrm{O-Ti}} = 1.7$ Å, $d_{\mathrm{Ti-N}} = 0.7$ Å, and $d_{\mathrm{N-C}} = 0.3$ Å, which agrees rather well with the gas phase values derived by DFT (within the expected experimental uncertainties, see also figure 1). Hence, the second-layer molecules are not significantly deformed. Their adsorption height is slightly higher than 6 Å, so that the resulting interlayer distance is in the range of 3.2 Å (averaging the values obtained for carbon and nitrogen atoms), which is close to the sums of the corresponding van-der-Waals radii and indicates a physisorptive interlayer interaction.

3.5.3. Pair-potential calculations

In the last part of this section we would like to address the intriguingly high stability of the bilayer structure, which was indicated by the observed growth behavior (layer-by-layer for the first two molecular layers, bilayer-by-bilayer for thicker films, see section 3.2) and the formation of extremely large domains as observed in LEED (see section 3.5.1). We have therefore applied a pair potential approach which is able to estimate the interaction energies between molecules in any known geometry [63].

Within this approach, we calculate the intermolecular potential of two objects (molecules) A and B as the sum of the interaction potentials of every atom of object A with every atom of object B, as a function of the (three-dimensional) distance vector between the two objects. Hence, by performing grid calculations, potential maps for all relevant molecular arrangements can be obtained and preferred relative positions and orientations of the molecules can be identified on the basis of the minima in these maps. Our approach considers electrostatic as well as van-der-Waals interaction. It was successfully applied to describe the intermolecular interactions and lateral structure formation of systems exhibiting weak adsorbate–substrate interactions, as, e.g., tetracene/Ag(111) [8], PTCDA/Au(111) and CuPc/Au(111) [63], as well as for the heteromolecular adsorbate systems

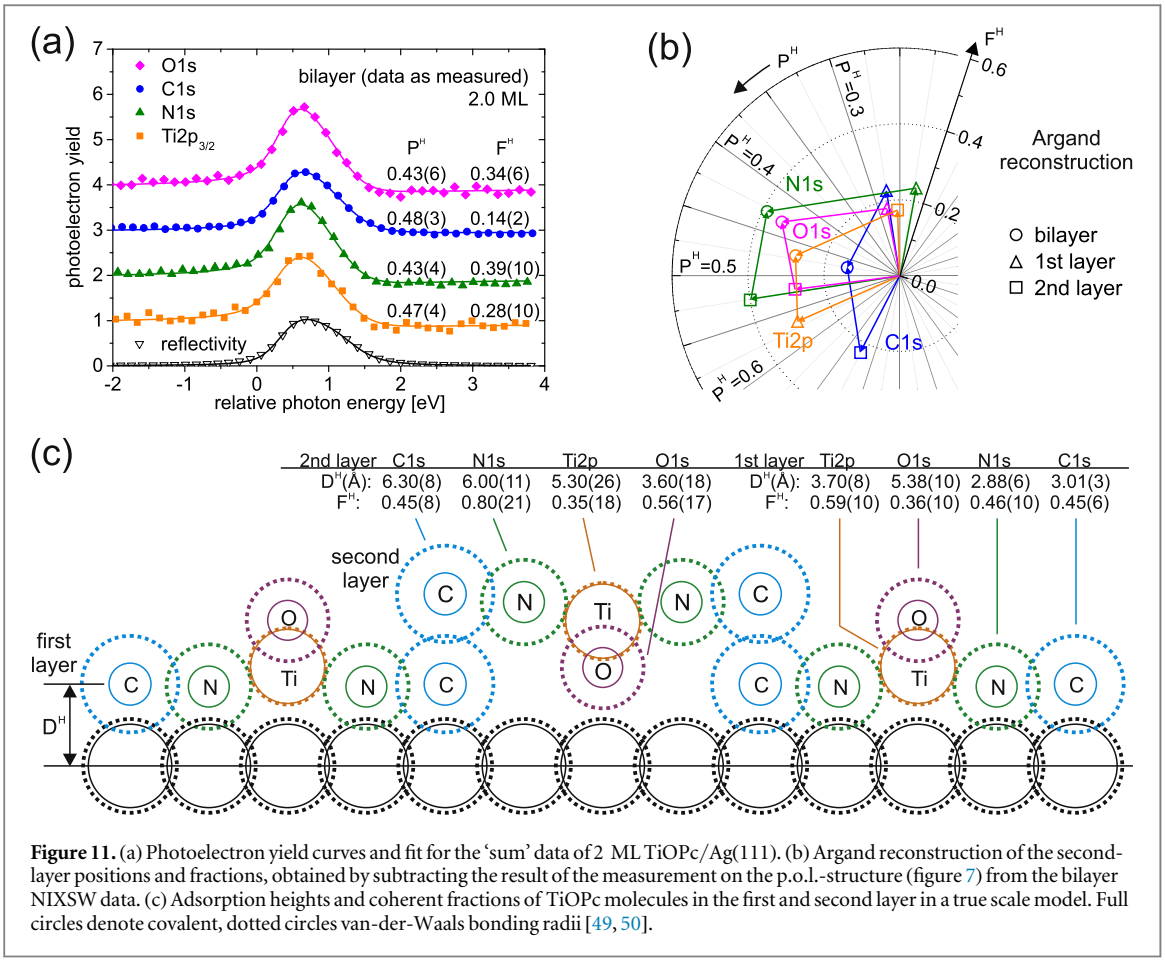

Figure 11. (a) Photoelectron yield curves and fit for the 'sum' data of 2 ML TiOPc/Ag(111). (b) Argand reconstruction of the second-layer positions and fractions, obtained by subtracting the result of the measurement on the p.o.l.-structure (figure 7) from the bilayer NIXSW data. (c) Adsorption heights and coherent fractions of TiOPc molecules in the first and second layer in a true scale model. Full circles denote covalent, dotted circles van-der-Waals bonding radii [49, 50].

F_{16}CuPc/CuPc/Ag(111) [64] and PTCDA+CuPc/Ag(111) [65]. The interaction between the two TiOPc layers for the system under study should therefore be well described by this approach. For further details and the parameter sets used for the atomic species in question see [63].

The lateral geometry, in particular the unit cell size and the in-plane orientation of the molecules in the bilayer structure, are well known from SPA-LEED and STM results (see figures 10(b) and (c)). We therefore performed calculations for the structure shown in figure 12(a): object A is one second-layer molecule TiOPc in TiO-down geometry. Object B consists of four TiO-up molecules which are positioned as in the first adsorbate layer, i.e., at the corners of a $\begin{pmatrix} 4.74 & 0 \\ 2.74 & 5.47 \end{pmatrix}$ unit cell. The intramolecular geometry of the molecules is assumed to be undistorted (compared to free molecules as calculated from DFT), and their in-plane orientation complies with the STM measurements shown in figure 10(d). We then performed a three-dimensional grid calculation varying the distance vector $(\Delta x,\ \Delta y,\ \Delta z)$ between the centers of both objects in the full range between $\Delta x,\ \Delta y = -25 \ldots 25$ Å and $\Delta z = -2.7 \ldots 3.5$ Å. In z-direction the center of the objects is defined by the position (height) of the nitrogen atoms.

Figures 12(b) and (d) show horizontal and vertical cuts, respectively, through the full 3D data cube at the position of the global minimum at (0, 0, 2.8 Å). In (c) the pair potential is plotted versus the vertical component Δz of the distance vector along a line through the minimum. This plot reflects depth and position of the potential minimum: $E = -3.9$ eV at $\Delta z = 2.8$ Å. Compared to other similar systems this indicates a very high energy gain for the formation of this molecular arrangement, the origin of which is mainly the electrostatic interaction of the alternating 'TiO-up/TiO-down' molecules representing an checkerboard pattern of oppositely oriented vertical dipole moments. Note that regarding interlayer distances, these theoretical results are in very good agreement with the NIXSW study reported above. For nitrogen, calculated and measured vertical distances are 2.8 Å and 3.1 Å, respectively, for carbon the corresponding values are 3.2 Å and 3.3 Å (see also figure 12(c)).

We can conclude that the large energy gain caused by the formation of this 'TiO-up/TiO-down' checkerboard structure is responsible for the high stability of the bilayer. It can explain the bilayer-by-bilayer growth for film thicknesses above two monolayers and the observed reorganization of the first-layer molecules upon adsorption of the second layer. The latter is reflected by the different unit cells of p.o.l.- and bilayer phase. But note that the bilayer interaction is not strong enough to suppress the formation of a first wetting layer for

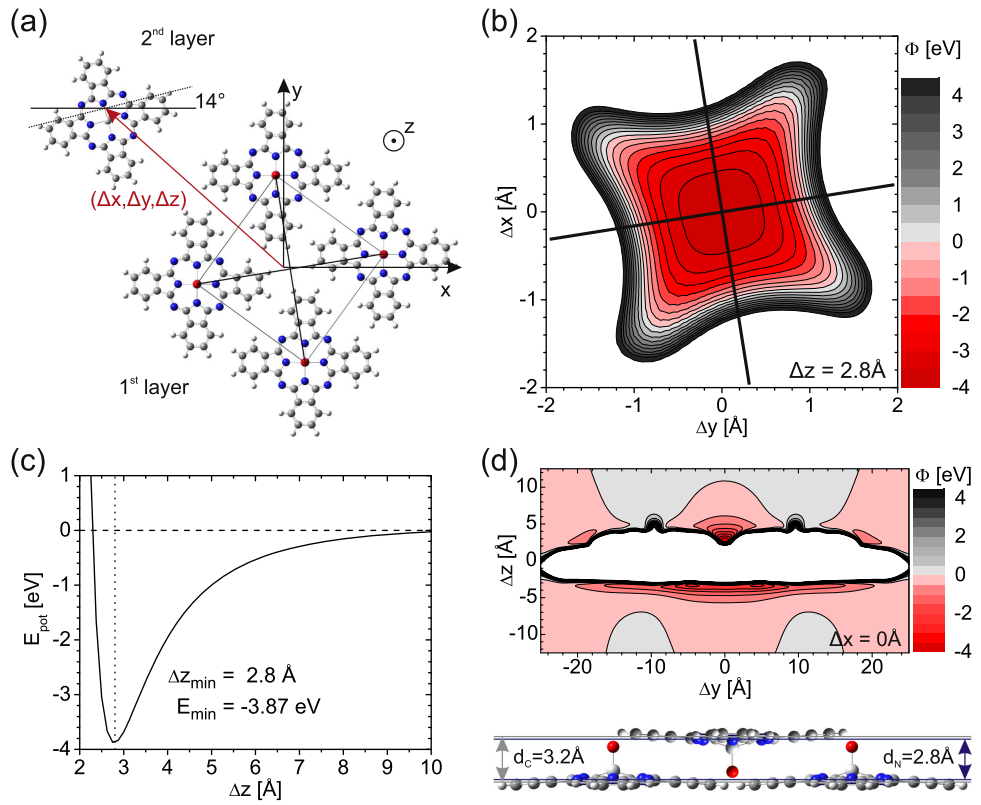

Figure 12. (a) Illustration of the objects A (second-layer molecule) and B (cluster of four first-layer molecules) and their relative orientation in the pair potential calculations. The red arrow represents the dislocation vector (Δx, Δy, Δz) which is varied in the grid calculations. The first-layer molecules are positioned on the bilayer unit cell grid as obtained from SPA-LEED, all molecular inplane orientations correspond to STM results. (b) Lateral and (d) vertical cut through the global minimum at (0, 0, 2.8Å) of the 3D data cube representing the result of the pair potential calculations. (c) Pair potential plotted versus Δz along a line through the global minimum indicating its depth of −3.9 eV.

(sub-)monolayer coverages. This indicates that the interaction of the first-layer molecules with the silver substrate, which is a chemisorptive interaction dominated by the π-system of the aromatic body of the molecule, is stronger than the electrostatic interaction between the first and the second adsorbate layer.

4. Summary

We have investigated the submonolayer and multilayer growth of TiOPc on Ag(111) using SPA-LEED, STM, HREELS, NIXSW, UPS and pair potential calculations. Similar to the adsorption of other metal-phthalocyanine molecules on Ag(111) we find three distinct phases in the submonolayer regime. At low coverages a disordered gas-like phase (g-phase) and a commensurate c_2-phase exists at RT and LT, respectively. At higher coverages we find a series of long-range ordered structures within the regime of the p.o.l.-phase, which exhibits a continuously shrinking unit cell with increasing coverage. The critical coverage for the phase transition from the g-/c_2- to the p.o.l.-phase lies between 0.5 and 0.93 ML, depending on the temperature.

In work function measurements and NIXSW we found that in the p.o.l.-phase the molecules adsorb uniformly in a 'TiO-up' configuration, i.e., with the Ti–O group pointing towards the vacuum. This adsorption configuration leads to the formation of a strong dipole layer when the first molecular layer is closing, which is well visible in the work function measurements. The dipole layer is stabilized by the chemisorption of the molecules on the Ag(111) surface, as indicated by charge transfer from the Ag(111) substrate to the LUMO of TiOPc visible in UPS, and by the adsorption heights obtained in NIXSW, which are well below van der Waals distances. This aspect, as well as the qualitative shape of the submonolayer phase diagram, is very similar to related systems like CuPc/Ag(111) [26], H_2Pc/Ag(111) [28] and SnPc/Ag(111) [13]. It demonstrates that for all Phthalocyanines the aromatic π-system is the decisive interaction channel between the first molecular layer and the Ag(111) surface. It was previously shown for H_2Pc/Ag(111) [28] that the nitrogen atoms contribute significantly to this interaction. In the case of TiOPc adsorption a strong IDCT also contributes to the interaction, as observed in HREELS from in-planes modes strongly involving the tetraazaporphyrine ring.

Above a coverage of 1 ML the molecules adsorb in a 'TiO-down' orientation until the second layer is closed. As shown by pair potential calculations, it is a rather strong Coulomb interaction between the (oppositely oriented) molecular dipole moments of the molecules in first and second layer which stabilizes this bilayer structure. This cancels out the dipole moment of the first dipole layer, which again is visible in work function measurements. NIXSW and STM data confirmed this molecular orientation, and gave insight in vertical adsorption heights, inter-layer distances and inplane orientations of the molecules. Thicker films are then growing in a bilayer-by-bilayer fashion, since the dipole-dipole interaction of the 'TiO-up/TiO-down' configuration within such a bilayer is very stable and enables a more efficient reduction of the surface energy than the adsorption of single layers of molecules, which would only physisorb on the underlying molecular film. This rule of bilayer-formation, which is only broken for the adsorption of the very first molecular layer due to its direct chemisorption on the Ag(111) surface, is the decisive difference to the growth of other phthalocyanine molecules with a smaller (or vanishing) vertical dipole moment (as, e.g., CuPc, H_2Pc and SnPc).

Acknowledgments

We thank Felix Erfurth, Andreas Stahl, Florian Pollinger, Yanyu Mi and Jörg Zegenhagen for their assistance during the NIXSW measurements, Christa Elsaesser for supporting the STM measurements and Christoph Kleimann, Marc Häming and Johannes Ziroff for helpful discussions. We acknowledge financial support from the Deutsche Forschungsgemeinschaft (KU 1531/2-1).

References

[1] Gottfried J M 2015 Surface chemistry of porphyrins and phthalocyanines *Surf. Sci. Rep.* **70** 259–379
[2] Ueno N and Kera S 2008 Electron spectroscopy of functional organic thin films: deep insights into valence electronic structure in relation to charge transfer properties *Prog. Surf. Sci.* **83** 490–557
[3] Zahn D R T, Gavrila G N and Salvan G 2007 Electronic and vibrational spectroscopies applied to organic/inorganic interfaces *Chem. Rev.* **107** 1161–232
[4] Tautz F S 2007 Structure and bonding of large aromatic molecules on noble metal surfaces: the example of PTCDA *Prog. Surf. Sci.* **82** 479–520
[5] Hill I G, Milliron D, Schwartz J and Kahn A 2000 Organic semiconductor interfaces: electronic structure and transport properties *Appl. Surf. Sci.* **166** 354–62
[6] Schreiber F 2000 Structure and growth of self-assembling monolayers *Prog. Surf. Sci.* **65** 151
[7] Forrest S R 1997 Ultrathin organic films grown by organic molecular beam deposition and related techniques *Chem. Rev.* **97** 1793–896
[8] Soubatch S, Kröger I, Kumpf C and Tautz F S 2011 Structure and growth of tetracene on Ag(111) *Phys. Rev.* B **84** 195440
[9] Stadtmüller B, Schröder S and Kumpf C 2015 Heteromolecular metal-organic interfaces: electronic and structural fingerprints of chemical bonding *J. Electron Spectrosc. Relat. Phenom.* **204 A** 80
[10] Pfuetzner S *et al* 2011 The influence of substrate heating on morphology and layer growth in C_{60}:ZnPc bulk heterojunction solar cells *Org. Electr.* **12** 435–41
[11] Fraxedas J *et al* 2011 Modulation of surface charge transfer through competing long-range repulsive versus short-range attractive interactions *J. Phys. Chem.* C **115** 18640–8
[12] Huang H, Chen W, Chen S, Qi D C, Gao X Y and Wee A T S 2009 Molecular orientation of CuPc thin films on C_{60}/Ag(111) *Appl. Phys. Lett.* **94** 163304
[13] Stadler C, Hansen S, Kröger I, Kumpf C and Umbach E 2009 Tuning intermolecular interaction on long-range ordered submonolayer organic films *Nat. Phys.* **5** 153–8
[14] Duhm S, Gerlach A, Salzmann I, Bröker B, Johnson R L, Schreiber F and Koch N 2008 PTCDA on Au(111), Ag(111) and Cu(111): Correlation of interface charge transfer to bonding distance *Org. Electron.* **9** 111–8
[15] Mannsfeld S and Fritz T 2005 Understanding organic–inorganic heteroepitaxial growth of molecules on crystalline substrates: experiment and theory *Phys. Rev.* B **71** 235405
[16] Willenbockel M, Lüftner D, Stadtmüller B, Koller G, Kumpf C, Soubatch S, Puschnig P, Ramsey M G and Tautz F S 2015 The interplay between interface structure, energy level alignment and chemical bonding strength at organic-metal interfaces *Phys. Chem. Chem. Phys.* **17** 1530–48
[17] Peisert H, Uihlein J, Petraki F and Chassé T 2015 Charge transfer between transition metal phthalocyanines and metal substrates: the role of the transition metal *J. Electron Spectrosc. Relat. Phenom.* **204A** 49–60
[18] Yamane H, Gerlach A, Duhm S, Tanaka Y, Hosokai T, Mi Y Y, Zegenhagen J, Koch N, Seki K and Schreiber F 2010 Site-specific geometric and electronic relaxations at organic-metal interfaces *Phys. Rev. Lett.* **105** 046103
[19] Kera S, Yabuuchi Y, Yamane H, Setoyama H, Okudaira K K, Kahn A and Ueno N 2004 Impact of an interface dipole layer on molecular level alignment at an organic-conductor interface studied by ultraviolet photoemission spectroscopy *Phys. Rev.* B **70** 085304
[20] Kera S, Abduaini A, Aoki M, Okudaira K K, Ue N, Harada Y, Shirota Y and Tsuzuki T 1998 Characterization of ultrathin films of titanyl phthalocyanine on graphite: PIES and UPS study *Thin Solid Films* **327-329** 278–82
[21] Kera S, Yamane H, Fukagawa H, Hanatani T, Okudaira K K, Seki K and Ueno N 2007 Angle resolved UV photoelectron spectra of titanyl phthalocynine monolayer film on graphite *J. Electron Spectrosc. Relat. Phenom.* **156** 135–8
[22] Kera S, Abduaini A, Aoki M, Okudaira K K, Ueno N, Harada Y, Shirota Y and Tsuzuki T 1998 Penning ionization electron spectroscopy of titanyl phthalocyanine ultrathin films: electronic state and molecular orientation *J. Electron Spectrosc. Relat. Phenom.* **88** 885–9
[23] Fukagawa H, Yamane H, Kera S, Okudaira K K and Ueno N 2006 Experimental estimation of the electric dipole moment and polarizability of titanyl phthalocyanine using ultraviolet photoelectron spectroscopy *Phys. Rev.* B **73** 041302
[24] Frisch M J *et al* 2004 *Gaussian 03 Revision C.02* (Wallingford, CT: Gaussian, Inc.)

[25] Stadler C, Hansen S, Pollinger F, Kumpf C, Umbach E, Lee T L and Zegenhagen J 2006 Structural investigation of the adsorption of SnPc on Ag(111) using normal-incidence x-ray standing waves *Phys. Rev.* B **74** 035404
[26] Kröger I *et al* 2010 Submonolayer growth of copper-phthalocyanine on Ag(111) *New J. Phys.* **12** 083038
[27] Kröger I, Stadtmüller B, Kleimann C, Rajput P and Kumpf C 2011 Normal incidence x-ray standing wave study on copper-phthalocyanine submonolayers on Cu(111) and Au(111) *Phys. Rev.* B **83** 195414
[28] Kröger I, Bayersdorfer P, Stadtmüller B, Kleimann C, Mercurio G, Reinert F and Kumpf C 2012 Submonolayer growth of H_2-Phthalocyanine on Ag(111) *Phys. Rev.* B **86** 195412
[29] Stadtmüller B, Kröger I, Reinert F and Kumpf C 2011 Submonolayer growth of CuPc on noble metal surfaces *Phys. Rev.* B **83** 085416
[30] Gerlach A, Hosokai T, Duhm S, Kera S, Hofmann O T, Zojer E, Zegenhagen J and Schreiber F 2011 Orientational ordering of nonplanar phthalocyanines on Cu(111): strength and orientation of the electric dipole moment *Phys. Rev. Lett.* **106** 156102
[31] Stahl U, Gador D, Soukopp A, Fink R and Umbach E 1998 Coverage-dependent superstructures in chemisorbed NTCDA monolayers: A combined LEED and STM study *Surf. Sci.* **414** 423–34
[32] Puschnig P, Berkebile S, Fleming A J, Koller G, Emtsev K, Seyller T, Riley J D, Ambrosch-Draxl C, Netzer F P and Ramsey M G 2009 Reconstruction of molecular orbital densities from photoemission data *Science* **326** 702–6
[33] Ziroff J, Forster F, Schöll A, Puschnig P and Reinert F 2010 Hybridization of organic molecular orbitals with substrate states at interfaces: PTCDA on silver *Phys. Rev. Lett.* **104** 233004
[34] Reinert F, Nicolay G, Schmidt S, Ehm D and Hüfner S 2001 Direct measurements of the L-gap surface states on the (111) face of noble metals by photoelectron spectroscopy *Phys. Rev.* B **63** 115415
[35] Batterman B W 1964 Dynamical diffraction of x-rays by perfect crystals *Rev. Mod. Phys.* **3** 682–717
[36] Lee J J, Fisher C J, Woodruff D P, Roper M G, Jones R G and Cowie B C C 2001 Non-dipole effects in photoelectron-monitored x-ray standing wave experiments: characterisation and calibration *Surf. Sci.* **494** 166–82
[37] Woodruff D P 1998 Normal incidence x-ray standing wave determination of adsorbate structures *Prog. Surf. Sci.* **57** 1–60
[38] Vartanyants I A and Zegenhagen J 1999 Photoelectric scattering from an x-ray interference field *Solid State Commun.* **113** 299–320
[39] Zegenhagen J 1993 Surface-structure determination with x-ray standing waves *Surf. Sci. Rep.* **18** 199–271
[40] Stadler C, Hansen S, Schöll A, Lee T-L, Zegenhagen J, Kumpf C and Umbach E 2007 Molecular distortion of NTCDA upon adsorption on Ag(111): a normal incidence x-ray standing wave study *New J. Phys.* **9** 50
[41] DL_PHASE is available from http:/ccp3.ac.uk (Daresbury Laboratory, UK)
[42] Wei Y, Robey S W and Reutt-Robey J E 2008 Flux-selected titanyl phthalocyanine monolayer architecture on ag(111) *J. Phys. Chem.* C **112** 18537–42
[43] Ueno N, Kera S, Sakamoto K and Okudaira K K 2008 Energy band and electron-vibration coupling in organic thin films: photoelectron spectroscopy as a powerful tool for studying the charge transport *Appl. Phys.* A **92** 495–504
[44] Zou Y, Kilian L, Schöll A, Schmidt T, Fink R and Umbach E 2006 Chemical bonding of PTCDA on Ag surfaces and the formation of interface states *Surf. Sci.* **600** 1240–51
[45] Häming M, Scheuermann C, Schöll A, Reinert F and Umbach E 2009 Coverage dependent organic-metal interaction studied by high-resolution core level spectroscopy: SnPc (sub)monolayers on Ag(111) *J. Electron Spectrosc. Relat. Phenom.* **174** 59–64
[46] Bendounan A, Forster F, Schöll A, Batchelor D, Ziroff J, Umbach E and Reinert F 2007 Electronic structure of 1 ml ntcda/ag(111) studied by photoemission spectroscopy *Surf. Sci.* **601** 4013–7
[47] Ishii H, Sugiyama K, Ito E and Seki K 1999 Energy level alignment and interfacial electronic structures at organic/metal and organic/organic interfaces *Adv. Mater.* **11** 605–25
[48] Hipps K W, Lu X, Wang X D and Mazur U 1996 Metal d-orbital occupation-dependent images in the scanning: tunneling microscopy of metal phthalocyanines *J. Phys. Chem.* **100** 11207–10
[49] www.webelements.com
[50] Bondi A 1964 Van der Waals volumes and radii *J. Phys. Chem.* **68** 441
[51] Hauschild A, Karki K, Cowie B C C, Rohlfing M, Tautz F S and Sokolowski M 2005 Molecular distortions and chemical bonding of a large pi-conjugated molecule on a metal surface *Phys. Rev. Lett.* **94** 036106
[52] Hauschild A, Temirov R, Soubatch S, Bauer O, Schöll A, Cowie B C C, Lee T-L, Tautz F S and Sokolowski M 2010 Normal-incidence x-ray standing-wave determination of the adsorption geometry of PTCDA on Ag(111): comparison of the ordered room-temperature and disordered low-temperature phases *Phys. Rev.* B **81** 125432
[53] Baran J D, Larsson J A, Woolley R A J, Cong Y, Moriarty P J, Cafolla A A, Schulte K and Dhanak V R 2010 Theoretical and experimental comparison of SnPc, PbPc, and CoPc adsorption on Ag(111) *Phys. Rev.* B **81** 075413
[54] Liu Z, Zhang X, Zhang Y and Jiang J 2007 Theoretical investigation of the molecular, electronic structures and vibrational spectra of a series of first transition metal phthalocyanines *Spectrochim. Acta* A **67** 1232–46
[55] Shklover V, Tautz F S, Scholz R, Sloboshanin S, Sokolowski M, Schäfer J A and Umbach E 2000 Differences in vibronic and electronic excitations of PTCDA on Ag(111) and Ag(110) *Surf. Sci.* **454** 60–6
[56] Tautz F S, Sloboshanin S, Shklover V, Scholz R, Sokolowski M, Schäfer J A and Umbach E 2000 Substrate influence on the ordering of organic submonolayers: a comparative study of PTCDA on Ag(110) and Ag(111) using HREELS *Appl. Surf. Sci.* **166** 363–9
[57] Tautz F S, Eremtchenko M, Schäfer J A, Sokolowski M, Shklover V and Umbach E 2002 Strong electron-phonon coupling at a metal/organic interface: PTCDA/Ag(111) *Phys. Rev.* B **65** 125405
[58] Tautz F S, Eremtchenko M, Schäfer J A, Sokolowski M, Shklover V, Glockler K and Umbach E 2002 A comparison of the chemisorption behaviour of PTCDA on different Ag surfaces *Surf. Sci.* **502** 176–84
[59] Amsalem P, Giovanelli L, Themlin J M and Angot T 2009 Electronic and vibrational properties at the ZnPc/Ag(110) interface *Phys. Rev.* B **79** 235426
[60] Auerhammer J M, Knupfer M, Peisert H and Fink J 2002 The copper phthalocyanine/Au(100) interface studied using high resolution electron energy-loss spectroscopy *Surf. Sci.* **506** 333–8
[61] Manandhar K, Ellis T, Park K T, Cai T, Song Z and Hrbek J 2007 A scanning tunneling microscopy study on the effect of post-deposition annealing of copper phthalocyanine thin films *Surf. Sci* **601** 3623–31
[62] Stadtmüller B *et al* 2015 Modification of the PTCDA-Ag(111) bond by formation of a hetero-organic bilayer film *Phys. Rev.* B **91** 155433
[63] Kröger I, Stadtmüller B, Wagner C, Weiss C, Temirov R, Tautz F S and Kumpf C 2011 Modeling intermolecular interactions of physisorbed organic molecules using pair potential calculations *J. Chem. Phys.* **135** 234703
[64] Kleimann C, Stadtmüller B, Schröder S and Kumpf C 2014 Electrostatic interaction and commensurate registry at the heteromolecular F_{16}CuPc - CuPc interface *J. Phys. Chem.* C **118** 1652–60
[65] Stadtmüller B, Henneke C, Soubatch S, Tautz F S and Kumpf C 2015 Tailoring metal-organic hybrid interfaces: Heteromolecular structures with varying stoichiometry on Ag(111) *New J. Phys.* **17** 023046